

AN ABSTRACT OF THE THESIS OF

Hatice Dicle Öziş for the degree of Master of Science in

Electrical and Computer Engineering presented on August 27, 2001.

Title: An Efficient Modeling Approach for Substrate Noise Coupling
Analysis with Multiple Contacts in Heavily Doped CMOS Processes.

Abstract approved: 

Kartikeya Mayaram

A computationally efficient and accurate substrate noise coupling model for multiple contacts in heavily doped CMOS processes is presented and validated with simulations and experimental data. The model is based on Z parameters that are scalable with contact separation and size. This results in fast extraction of substrate resistances for large circuit examples. The Z -parameter model can be readily extracted from three dimensional simulations or measured data. Extensions of the model to lightly doped substrates are also presented. Several examples demonstrate that this approach can be orders of magnitude faster than currently available techniques for substrate resistance extraction. The computed substrate resistances are in close agreement with the numerical simulations, with a maximum error less than 10%.

©Copyright by Hatice Dicle Öziş

August 27, 2001

All Rights Reserved

An Efficient Modeling Approach for Substrate Noise
Coupling Analysis with Multiple Contacts
in Heavily Doped CMOS Processes

by

Hatice Dicle Öziş

A THESIS

submitted to

Oregon State University

in partial fulfillment of
the requirements for the
degree of

Master of Science

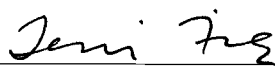
Completed August 27, 2001
Commencement June 2002

Master of Science thesis of Hatice Dicle Öziş presented on August 27, 2001

APPROVED:



Major Professor, representing Electrical and Computer Engineering

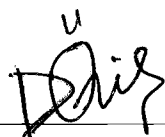


Head of the Department of Electrical and Computer Engineering



Dean of the Graduate School

I understand that my thesis will become part of the permanent collection of Oregon State University libraries. My signature below authorizes release of my thesis to any reader upon request.



Hatice Dicle Öziş, Author

ACKNOWLEDGMENT

Many people have contributed to the development of this thesis over the last two years. First and foremost I would like to thank my advisors, Dr. Karti Mayaram and Dr. Terri Fiez, for supporting this research and for providing an environment in which it has been possible to freely pursue independent avenues of thought. Their foresight, physical intuition, and integrity have been a constant and dependable guide throughout this entire work. I would also like to acknowledge the other members of my committee, Dr. Raghu Settaluri and Dr. Chih-hung Chang, both of whom have showed interest in my work. I am also thankful to them for taking the time and serving on my defense committee. I also would like to thank Dr. Raghu Settaluri for the discussions on Momentum.

I would like to thank CDADIC for supporting this work. I am also grateful to several industry members who have contributed to this project through their feedback at CDADIC meetings.

I firmly believe that the work environment makes the greater part of the learning experience and for this I would like to thank my colleagues in the AMS Group. I owe many thanks to Uma Chilakapati and Aline Sadate for their help in my arrival to US, Robert Batten for helping with the tools, software, and measurements, Anil Samavedam for his thesis, Radu and Christina Fetche, John McNitt for their help in my first semester at WSU, Cheng-gang Xu for his software EPIC, Robert Shreeve for his help on measurements, Ruoxin Jiang, Shanthi Bhagavatheeswaran, Oleg Mikulchenko, Yutao Hu, Yuxian Ou, Kalyan Ghatak, Madhu Chennam, Vinay Chandrasekhar, Xena Cummings, Edgard Yemelong Constand, Zhimin Li, Taras Dudar, Volodymyr Kratyuk, Ravikanth Suravarapu, Kannan Soundarapandian, Mohanalakshmi Koteeswaran, Prashanth Drakshapalli and Ragini Murugan for the

friendly and educational environment. I am thankful to Nathen Barton, Nilakantan Seshan, Xena Cummings and Robert Shreeve for proofreading my thesis and making valuable comments.

I am grateful to Nathen Barton for his friendship and countless favors he has done for me. I especially thank Aline Sadate and Nilakantan Seshan for their friendship and making lunch the high point of my day.

I am greatly indebted to all the teachers in my life including the first and the most important ones, my parents. My parents have been my role models since the early stages of my life. Without their, love, support, understanding, encouragement and sacrifices I wouldn't be here. I am thankful to my brother, for always being there for me, for his love and support. Last but not the least, my deepest gratitude and love belongs to my husband Mithat Unsal, for his unconditional love, support and superhuman patience.

TABLE OF CONTENTS

	<u>Page</u>
1 INTRODUCTION	1
2 MACROMODEL	3
3 EXTENSION OF MACROMODEL TO ARBITRARY MULTIPLE CON- TACTS	7
3.1 Shortcomings of the Current Model for Multiple Contacts	7
3.2 Proposed Solution to Obtain the Substrate Resistances	9
3.3 Substrate Coupling Analysis Using 2D Device Simulations	12
3.4 Extension of the Model to the Third Dimension	20
3.5 Model for Contacts with Different Sizes	25
4 PRELIMINARY MODEL FOR LIGHTLY DOPED CMOS SUBSTRATES	40
4.1 2D Simulations in Lightly Doped Substrates	40
4.2 Lightly Doped Substrate Modeling in 3D	42
5 APPLICATION EXAMPLES AND COMPUTATIONAL EFFICIENCY...	49
6 EXPERIMENTAL VERIFICATION	55
7 CONCLUSION	62
BIBLIOGRAPHY	63
APPENDICES	65

LIST OF FIGURES

<u>Figure</u>	<u>Page</u>
2.1 Resistive model for substrate coupling for two contacts.	5
3.1 Resistive substrate network for multiple contacts.	8
3.2 Substrate resistance values for (a) two identical contacts, and (b) three identical contacts. This example illustrates the need for using an alternate formulation instead of a resistance formulation.	8
3.3 Z parameters are defined as the ratio of the open circuit voltage at contact m to the source current at contact j for any arbitrary contacts j and m	9
3.4 The resistive substrate network for four contacts using: (a) a Z -parameter formulation and (b) a Y -parameter formulation.	10
3.5 Two-port Z parameters used for constructing an N-port Z matrix.	11
3.6 Cross section of a heavily doped substrate with point contacts.	13
3.7 Cross section of a lightly doped substrate with point contacts.	14
3.8 (a) Z_{11} vs. contact width. (b) $1/Z_{11}$ vs. contact width and its fit to a line.	15
3.9 Current flow lines illustrate nearby contact effects in a doped heavily substrate.	16
3.10 Logarithm of Z_{12} as a function of separation in heavily doped substrates. The two contacts are $5\mu m$ and $100\mu m$ wide.	18
3.11 Medici simulations show that β is independent of contact widths. In this figure β is the slope of the $\log(Z_{12})$ curve.	18
3.12 2D and 3D cross sections of a substrate with two contacts.	20
3.13 Substrate geometry for simulation of a heavily doped substrate in Momentum.	21
3.14 $1/Z_{11}$ versus width for square contacts comparing the model and simulations.	22

LIST OF FIGURES (Continued)

Figure	Page
3.15 The Z_{11} model is in good agreement with measurements from [6] and Momentum simulations.	23
3.16 3D simulation results showing Z_{11} dependence on nearby contacts. . .	23
3.17 Simulations and model for Z_{12} show that β is independent of contact sizes. The model and simulations are in good agreement.	25
3.18 Two contacts with different sizes.	26
3.19 Simulations and model for Z_{12} show that Z_{12} decays exponentially with increasing separation (x) between the contacts.	26
3.20 Simulations for $w = 100\mu m$ show that Z_{12} has a quadratic dependence on y when $x_0 = 35\mu m$. The maximum value of Z_{12} is at $y = 45\mu m$. . .	27
3.21 A large ($10\mu m \times 110\mu m$) and small ($10\mu m \times 10\mu m$) contact for three different relative positions. The value of Z_{11} is constant for a fixed area and perimeter. Since the Z_{11} (α) value is independent of y , parameters a , b and c are scalable with contact dimensions.	28
3.22 two contacts of size ($10\mu m \times 110\mu m$) and ($110\mu m \times 10\mu m$) for two different relative positions at zero separation ($x = 0$). The value of Z_{11} is constant for a fixed area and perimeter. This example verifies that the parameters a , b and c are scalable with contact dimensions.	29
3.23 Model predicts the simulation results for Z_{12} for variations in x and y	30
3.24 An example of an L-shape and square contact illustrating two sided coupling.	31
3.25 The model and simulations are in agreement for the contacts in Fig. 3.24 for (a) $x_0 = 30\mu m$, (b) different x_0 values. The L-shaped contact consists of two $10\mu m \times 100\mu m$ rectangles and the square contact is $10\mu m \times 10\mu m$	32
3.26 3D Z_{12} plot and the constant Z_{12} contour lines show the coupling between the contacts in Fig. 3.24: (a) 3D Z_{12} plot. (b) Constant Z_{12} contours.	34

LIST OF FIGURES (Continued)

<u>Figure</u>	<u>Page</u>
3.27 Illustration of the movement of the small contact along one of the contour lines shown in Fig. 3.26 (b).	35
3.28 The model also works for asymmetric geometries. (a) An asymmetric L-shaped contact and a square contact. (b) Model agrees with the simulation results for different y values for the contact geometries of (a) with a maximum error of 12.6 %.	36
3.29 (a) A U-shaped and a square contact. (b) The square contact is completely surrounded by another contact.	37
3.30 The model and simulations agree for the contact geometry in Fig. 3.29 (a). (a) Logarithm of Z_{12} versus y for three different x_0 values obtained by using the model. (b) Logarithm of Z_{12} versus x_0 when $y = 40\mu m$. In this example the U-shaped contact consists of three rectangular contacts of size $100\mu m \times 10\mu m$, and the square contact is $10\mu m \times 10\mu m$	38
3.31 (a) The model agrees with simulations for the contacts shown in Fig. 3.29 (b) when $x_0 = 40\mu m$. (b) 3D plot of Z_{12} shows that the minimum value of Z_{12} occurs in the middle of the surrounding contact. The square contact consists of four rectangular contacts of size $100\mu m \times 10\mu m$, where the square contact is $10\mu m \times 10\mu m$	39
4.1 Current flow lines in a lightly doped substrate for a point contact in: (a) substrate with a channel-stop implant layer and (b) a homogeneous substrate.	41
4.2 Z_{11} as a function of contact width.	42
4.3 Logarithm of Z_{12} as a function of separation between the injecting and sensing contacts in a lightly doped substrate.	43
4.4 Simulations show that Z_{11} has a strong dependence on die area for a given contact size in lightly doped CMOS processes.	44
4.5 Z_{11} does not depend on die area for a given contact size in heavily doped CMOS processes.	45

LIST OF FIGURES (Continued)

<u>Figure</u>	<u>Page</u>
4.6 Simulations show that Z_{11} depends on contact size for a constant die area of $(1.2mm \times 0.24\mu m)$. This result cannot be predicted by 2D device simulations.	45
4.7 Z_{11} is a function of contact size for a constant die area of $(1mm \times 1mm)$. EPIC simulation results agree with the SCA simulations.	46
4.8 Logarithm of Z_{12} in lightly doped substrates. 3D simulation results are obtained from EPIC.	47
4.9 Simulations show that Z_{12} can be modeled as a modified Bessel function of the 0^{th} order. Model and the simulations are in good agreement. In this example the contacts are $2\mu m \times 2\mu m$ and the chip area is $(1mm \times 0.25mm)$	48
5.1 Calculation of substrate resistance networks comparing the conventional and the scalable modeling approaches. (a) Two large contacts are discretized into panels and the calculated cross-coupling resistance value for a separation of $40\mu m$ is $22.2K\Omega$. (b) For the scalable model the contacts are not discretized into panels. The calculated resistance value is $21.7K\Omega$	50
5.2 Verification of the model for different contact shapes for a separation $x = 40\mu m$	50
5.3 A three contact example is used to show the application of the scalable model to multiple contacts.	51
5.4 A non-scalable substrate model requires division of contacts into small panels.	53
6.1 Substrate coupling test structures.	55
6.2 Measured data for Z_{11} agrees with the results obtained from the model.	56
6.3 Different contact geometries. Measurement results show that the area and perimeter dependent Z_{11} model also predicts the measured values accurately for these different shapes.	58
6.4 (a) Array structure for $2.4\mu m \times 2.4\mu m$ contacts. (b) Z_{12} measurement results agree with the model for contacts of (a).	59

LIST OF FIGURES (Continued)

<u>Figure</u>		<u>Page</u>
6.5	At zero separation the two $2.4\mu m \times 2.4\mu m$ contacts merge into a single contact of size $4.8\mu m \times 2.4\mu m$	59
6.6	Three different sized contact pairs at a separation of $10\mu m$	60
6.7	The modeled and extracted values of α are in good agreement.	61

LIST OF TABLES

<u>Table</u>		<u>Page</u>
3.1	R_{12} values calculated from the Z -parameter-based model compared with the values obtained from MEDICI simulations.	19
5.1	Comparison of resistance values obtained from simulations and the scalable model for the example in Fig. 5.1.	50
5.2	Comparison of resistance values obtained from simulations and the scalable model for the example in Fig. 5.2.	51
5.3	Resistance values from simulations and the scalable model are in good agreement for the example in Fig. 5.3.	52
5.4	Size of Z matrices for the scalable model and panel-based approaches.	53

LIST OF APPENDICES

<u>Appendix</u>	<u>Page</u>
A Calculation of Z Parameters from S Parameters	66
B Model Parameter Extraction for Z_{11}	67
C Model Parameter Extraction for Z_{12}	70
D Cadence Affirma Substrate Coupling Analysis	76
E Measurement Structures on the Test Chip.....	78

AN EFFICIENT MODELING APPROACH FOR SUBSTRATE NOISE COUPLING ANALYSIS WITH MULTIPLE CONTACTS IN HEAVILY DOPED CMOS PROCESSES

1. INTRODUCTION

With the continued scaling of CMOS processes, it is possible to integrate digital, analog and RF circuitry on a single chip. The digital circuits inject noise that is sensed by the sensitive analog and RF blocks through the common substrate. This noise coupling from the substrate can severely degrade the performance of noise sensitive circuits. For this reason, it is essential that substrate noise coupling analysis is included in the design flow of integrated circuits. Furthermore, this analysis must be accurate and efficient for large designs.

The increasing importance of substrate noise coupling in integrated circuits has resulted in many studies on this topic. At present several numerical techniques are available for substrate noise coupling [1]- [4] and [11]. These approaches, however, can only be used after the final layout has been done. A large resistive substrate network is extracted for low frequency applications [17] and included in circuit simulations. Model-order reduction techniques are used to reduce the size of the substrate network [1] and [5], but these techniques continue to be computationally expensive for full-chip substrate noise analysis. An alternate approach has been pursued in [6]

and [12] where simple scalable macromodels have been used for efficient substrate resistance extraction.

In [6], a scalable design-oriented macromodel was presented that predicts substrate noise coupling between blocks based on their separation and size. This macromodel makes it possible for designers to simulate the effects of substrate noise in a circuit during the design phase. The model was developed for heavily doped substrates.

In this thesis, the focus is on an efficient macromodel for substrate noise coupling in heavily and lightly doped CMOS substrates. This model is an extension and reformulation of the model proposed in [6] and has been extensively validated with device simulations, electromagnetic simulations and measured data. The model has significantly better computational efficiency and accuracy than [12].

The thesis is organized as follows. The macromodel of [6] is briefly described in Section 2. The substrate model for two contacts is then extended to multiple contacts and arbitrary shapes by eliminating the drawbacks of the previous macromodel in Section 3. A preliminary model for lightly doped substrates is proposed in Section 4. Applications of the model and its computational efficiency are demonstrated in Section 5. Experimental verification of the model is given in Section 6. Conclusions and future work are provided in Section 7.

2. MACROMODEL

Currently the most commonly used method to resolve substrate noise coupling problems is a very costly trial-and-error procedure due to the lack of an efficient substrate network extractor for practical circuits. This delays IC designs and increases engineering time. Many techniques have been proposed for substrate network computation.

Several results have been published with detailed numerical analyses of substrate noise coupling. In [1], [2] and [8] device simulators were used for a full numerical simulation of currents and potentials in the substrate. A simplified substrate equation can be obtained by solving the Poisson's and current continuity equations in the substrate. The partial differential equations are usually solved by difference equations and the finite difference method is a popular method. In this method the entire substrate is discretized or meshed. The resulting resistance and capacitance matrices are very large but sparse. For these numerical techniques, the mesh definition plays a key role, since there is a tradeoff between accuracy and computational efficiency. In general, it is not possible to obtain accurate results using the traditional numerical techniques for large circuits.

Another method to calculate the substrate network is the boundary element method (BEM). The boundary element methods [2], [4] and [11] are based on the solution of the Green's function with appropriate boundary conditions. This method requires meshing only for the contacts and results in a small but dense Z matrix. In order to calculate substrate resistances, the inverse Z matrix has to be computed. Dense matrix inversion has a computational complexity of $O(N^3)$ where N is the matrix dimension. Hence this method is also computationally intensive for large problems.

In the BEM the major computational burden is the implementation of the Green's function directly, as a double Fourier series. Each entry in the dense BEM matrix requires a large number of multiplications. Usage of a two-dimensional discrete cosine transform (DCT), implemented efficiently with an FFT algorithm [10] can considerably improve the computational efficiency. But the method still has difficulty in handling problems with large numbers of contacts. The preprocessed BEM [9] is different from the ordinary boundary element methods in that Z parameters are obtained from polynomial curve fitting. This method provides a simpler estimation of Z parameters. Although the preprocessed boundary element method is not as computationally expensive as the previously described methods, models for different geometries and spacings need to be computed and stored in a design tool library.

The disadvantage of finite difference and direct boundary element techniques is that they are computationally expensive and complex and hence do not provide design insight. For preprocessed BEM, pre-characterized libraries have to be calculated in order to obtain models for different geometries. These libraries have to be changed each time the technology is updated. Consequently, these methods are not efficient for large and practical designs.

In [6] and [12], scalable macromodels for substrate resistances have been developed. In these methods the substrate resistances are scalable with contact dimensions, shape and separation, and therefore, can be easily calculated for a given process. Scalable models are reusable when a layout is changed. The previous macromodels were derived only for two contacts and cannot be readily used for multiple contacts.

The model of [6] was obtained based on device simulation results from TMA-Medici [13], a two-dimensional device simulator. Simulations have shown that a

simple resistive macromodel can be used to model the substrate up to 2-3 GHz accurately. In [6], the macromodel was developed for low frequencies and heavily doped CMOS substrates.

This work was extended in [7] to a model for lightly doped CMOS processes at low frequencies. A resistive two-port model is used to represent the substrate as shown in Fig. 2.1.

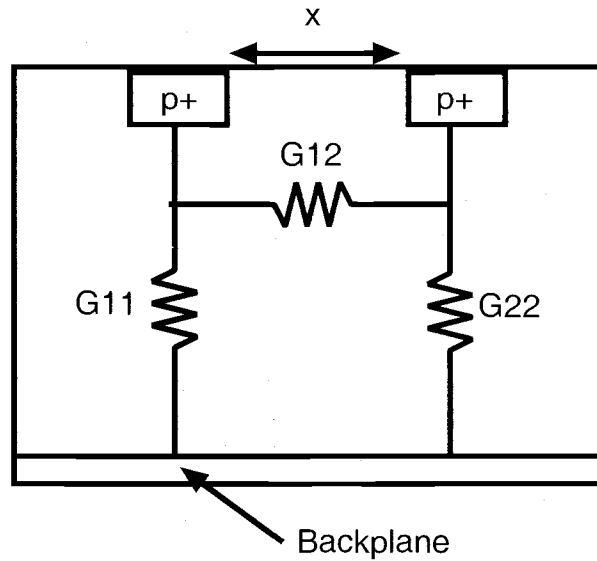


Figure 2.1. Resistive model for substrate coupling for two contacts.

The advantages of these macromodels over the previous techniques can be summarized as follows. These models are

- *Simple:* The models can be used for any contact size and separation and require only a few technology specific parameters.
- *Accurate:* The models predict the resistance values accurately.
- *Efficient:* The models can be used for arbitrary contact shapes and result in small dense Z matrices. This translates into computational efficiency.

- *Versatile:* The macromodels can be easily used for different layouts, since they are scalable and can be used with arbitrary contact shapes.
- *Intuitive:* The calculated resistive network gives insight into the coupling and isolation mechanisms on a substrate.

3. EXTENSION OF MACROMODEL TO ARBITRARY MULTIPLE CONTACTS

3.1. Shortcomings of the Current Model for Multiple Contacts

The substrate noise coupling macromodels of [6], [7] and [12] were developed for two contacts. The resistance values were extracted for a pi-network (Fig. 2.1) that includes a cross-coupling resistance between the contacts and resistances from the contact to the backplane. However, substrate noise coupling involves multiple contacts as illustrated in Fig. 3.1. From this figure, it can be seen that the overall substrate coupling resistance network is complex. Each pair of contacts has a resistance to the backplane as well as a cross-coupling resistance between each other. Therefore macromodels must incorporate multiple contacts. A straightforward approach would be the use of the two-port resistive model for multiple contacts. However this results in resistance values that are incorrect. As an example, consider a two-port resistive network formulation derived for a 3-contact case. The simulated resistance values for two identical contacts at a separation of $x = 10\mu m$ are shown in Fig. 3.2 (a). The addition of an identical third contact at $x = 10\mu m$ separation from both contacts alters the resistance values as shown by the simulated resistances in Fig. 3.2 (b). According to a simple resistance formulation method, the resistance values in Fig. 3.2 (b) should be identical to the values in Fig. 3.2 (a). However, this is not the case and an alternate formulation is required. This example demonstrates the shortcoming of extending the resistance-based macromodels [6], [7], and [12] directly to multiple contacts. Clearly, a reformulation of the original resistance-based model is required.

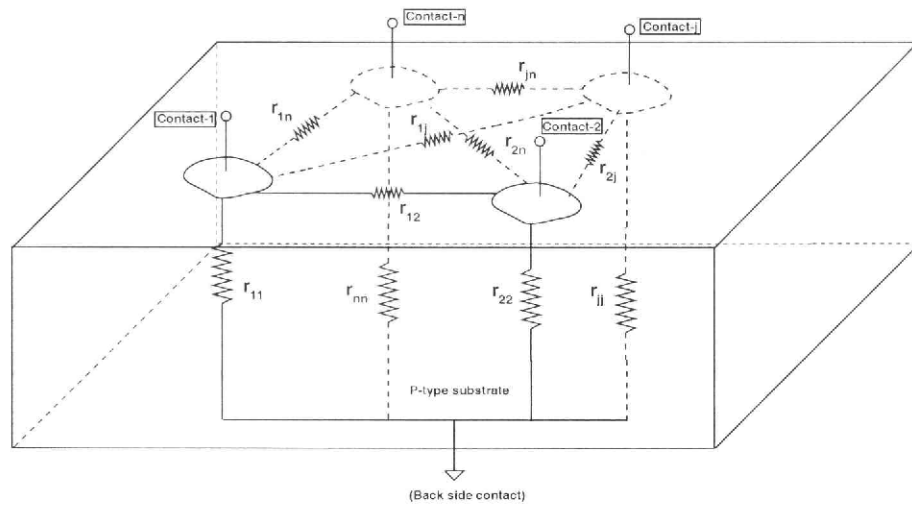


Figure 3.1. Resistive substrate network for multiple contacts.

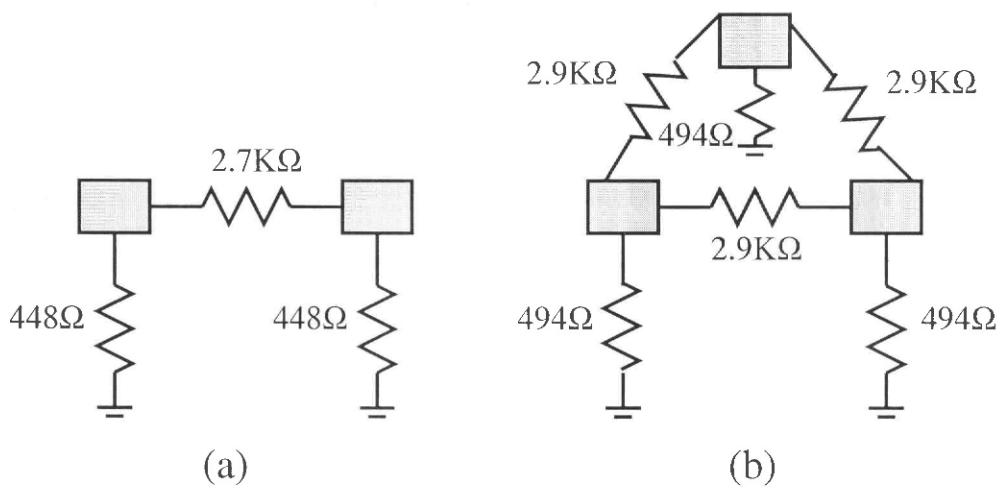


Figure 3.2. Substrate resistance values for (a) two identical contacts, and (b) three identical contacts. This example illustrates the need for using an alternate formulation instead of a resistance formulation.

3.2. Proposed Solution to Obtain the Substrate Resistances

The new formulation should be simple, accurate, scalable and intuitive as the resistance-based one. Moreover, it should include the effect of nearby contacts and predict the substrate resistance network accurately for any number of contacts. A macromodel in which the voltages at the contacts and the currents through them are related by scalable Z parameters satisfies all the above conditions. A model based on Z parameters allows accurate prediction of resistance values in the presence of nearby contacts. This is not the case for the resistance-based model.

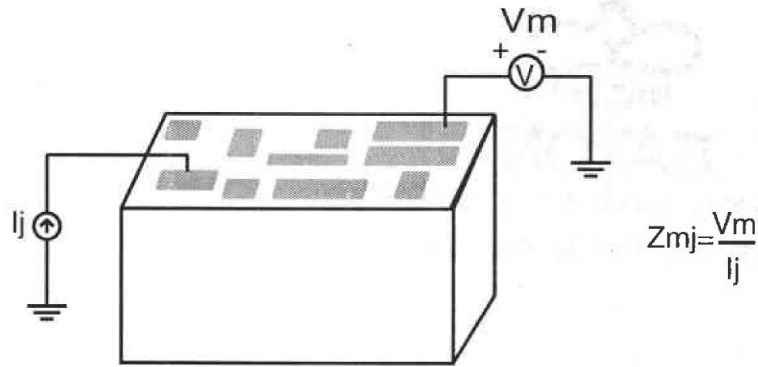


Figure 3.3. Z parameters are defined as the ratio of the open circuit voltage at contact m to the source current at contact j for any arbitrary contacts j and m .

Z parameters are open circuit parameters as shown in Fig. 3.3, accordingly the network under consideration stays the same for different Z -parameter measurements. The Z parameters for two contacts do not change due to other nearby contacts for large contact separations. Simulation results show that Z parameters stay constant for separations larger than $10\mu m$.

Although Y parameters are the dual of Z parameters, they cannot be used to formulate the substrate network. The Y parameters are short circuit parame-

ters, therefore for every Y -parameter measurement the substrate network is altered because of the grounded nodes. A Y -parameter formulation also does not take into account the cross-coupling resistances between two grounded nodes, and the resistances from grounded nodes to the backplane. Fig. 3.4 shows the difference between the resistive networks for Z -parameter and Y -parameter formulations for a four-contact example. In Fig. 3.4 (a) a Z -parameter formulation is shown where all resistances from the contacts to the backplane and cross-coupling resistances between them are present because of the open circuit measurements. In Fig. 3.4 (b) a Y -parameter formulation is shown. Resistors R_{22} , R_{33} , R_{44} , R_{23} and R_{34} are eliminated in the Y -parameter formulation as they are connected between grounded nodes.

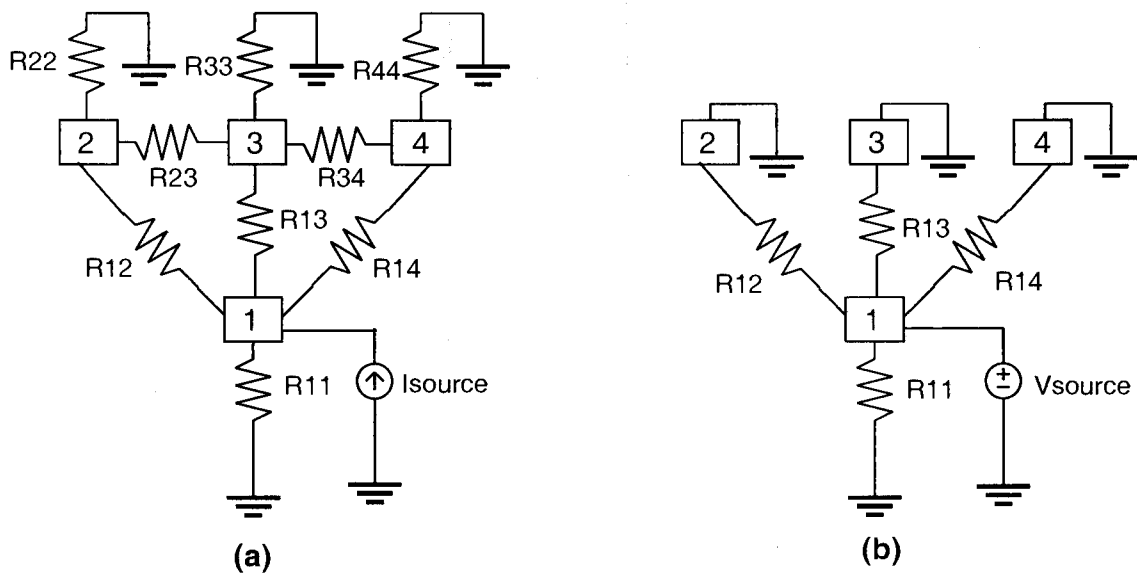


Figure 3.4. The resistive substrate network for four contacts using: (a) a Z -parameter formulation and (b) a Y -parameter formulation. In the Y -parameter formulation resistors R_{22} , R_{33} , R_{44} , R_{23} and R_{34} are eliminated as they are connected between grounded nodes.

Multiple contacts can be handled readily by using two-port Z parameters for the core model formulation. The process for an N -contact problem consists of the following steps:

1. The 2-port Z parameters are calculated using the size and separation information of contacts j and m . The matrix entries corresponding to the two contacts j and m , shown in Fig. 3.5, are given in Eq. (3.1).
2. The $N \times N$ Z matrix is constructed from the 2-port Z parameters by considering two contacts at a time. This procedure results in a dense $N \times N$ matrix when all contact pairs have been considered.
3. The resistance values are then calculated from the overall Z matrix, by inverting the Z matrix.

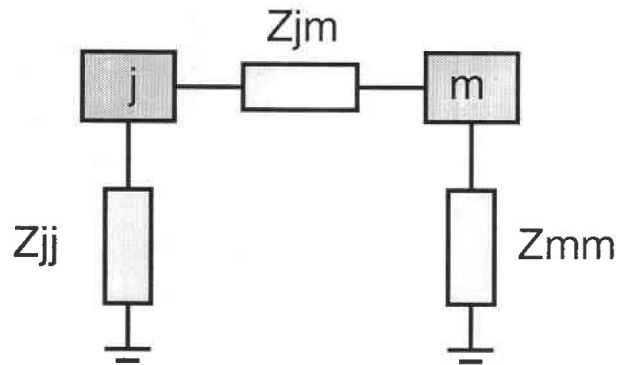


Figure 3.5. Two-port Z parameters used for constructing an N -port Z matrix.

$$Z = \begin{bmatrix} \cdot & \cdot & \cdot & \cdot & \cdot & \cdot & \cdot \\ \cdot & z_{jj} & \cdot & \cdot & z_{jm} & \cdot & \cdot \\ \cdot & \cdot & \cdot & \cdot & \cdot & \cdot & \cdot \\ \cdot & \cdot & \cdot & \cdot & \cdot & \cdot & \cdot \\ \cdot & \cdot & \cdot & \cdot & \cdot & \cdot & \cdot \\ \cdot & z_{jm} & \cdot & \cdot & z_{mm} & \cdot & \cdot \\ \cdot & \cdot & \cdot & \cdot & \cdot & \cdot & \cdot \\ \cdot & \cdot & \cdot & \cdot & \cdot & \cdot & \cdot \end{bmatrix} \quad (3.1)$$

3.3. Substrate Coupling Analysis Using 2D Device Simulations

Two-dimensional (2D) device simulations can be used to develop a model for substrate coupling. Device simulations are a convenient way of deriving the model because there are no measurement uncertainties. Furthermore, it is possible to do many controlled experiments with a simulator by changing the size and separation of injecting and sensing contacts. A 2D model provides insight into substrate coupling mechanisms for different fabrication processes. Device simulators provide accurate results and allow the user to define nonhomogeneous substrate layers such as p+ and n-well regions in a p- epi on p+ silicon substrate.

In order to derive the model, 2D simulations were performed using MEDICI [13]. The key information provided to MEDICI is the process information such as the doping concentrations and layer thicknesses, along with the size and separation of the injecting and sensing contacts. MEDICI generates current flow lines, equipotential lines and Y or Z parameters from the process information for a given separation and contact size. The cross section of the heavily and lightly doped processes are illustrated in Figs. 3.6 and 3.7, respectively.

The heavily doped substrate shows three distinct layers: a heavily doped p+ channel-stop implant, a lightly doped epi layer and a heavily doped p+ bulk region. The resistivities and thicknesses for these layers are shown in Fig. 3.6. The lightly doped substrate consists of two layers: a p+ channel-stop implant and an uniform lightly doped substrate, as shown in Fig. 3.7.

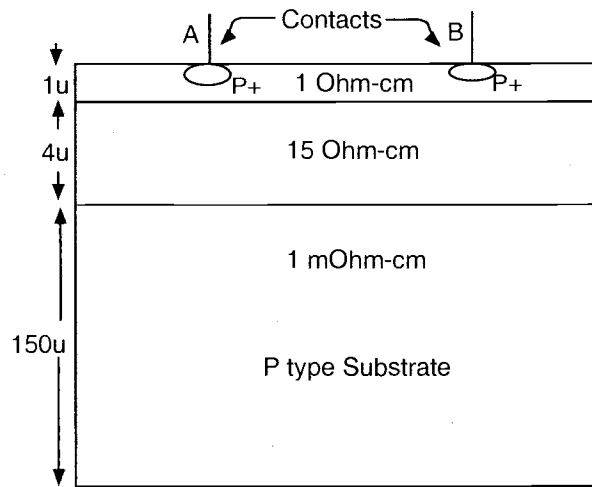


Figure 3.6. Cross section of a heavily doped substrate with point contacts.

The dependence of contact size for Z_{11} in heavily doped substrates is examined first. For a single contact case, the width of the contact is changed from $0.5\mu m$ to $80\mu m$ and Z_{11} values are obtained from MEDICI simulations. The plots of Z_{11} and $1/Z_{11}$ with respect to the contact widths are shown in Fig. 3.8.

From Fig. 3.8 (b) a linear relationship can be seen between $1/Z_{11}$ and contact width. This is confirmed by a linear form for $1/Z_{11}$ given by

$$\frac{1}{Z_{11}} = a + bw_1 \quad (3.2)$$

where a and b are process parameters that can be obtained from curve fitting. The values obtained for the substrate profile used in this particular simulation are:

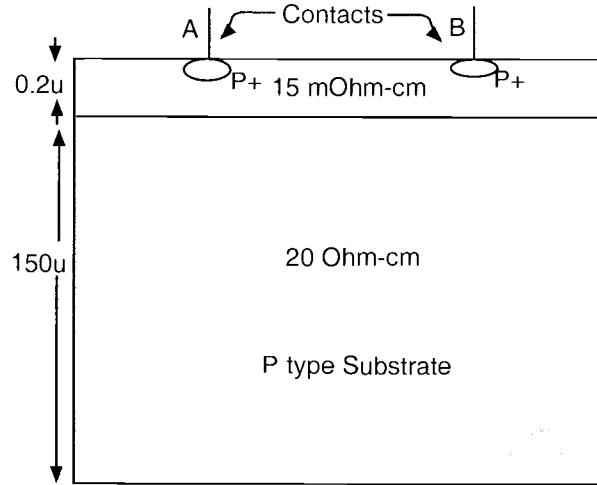
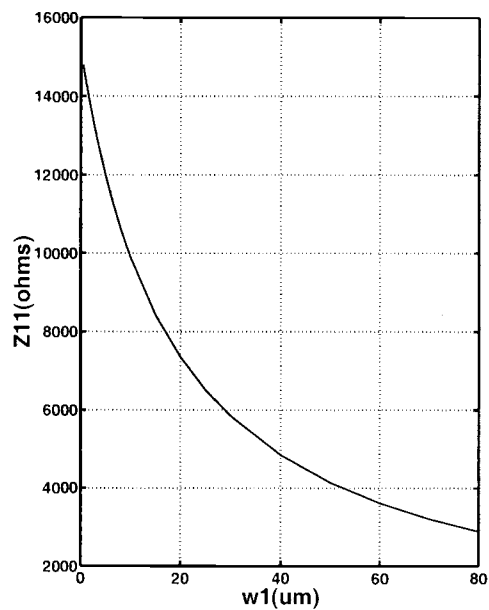


Figure 3.7. Cross section of a lightly doped substrate with point contacts.

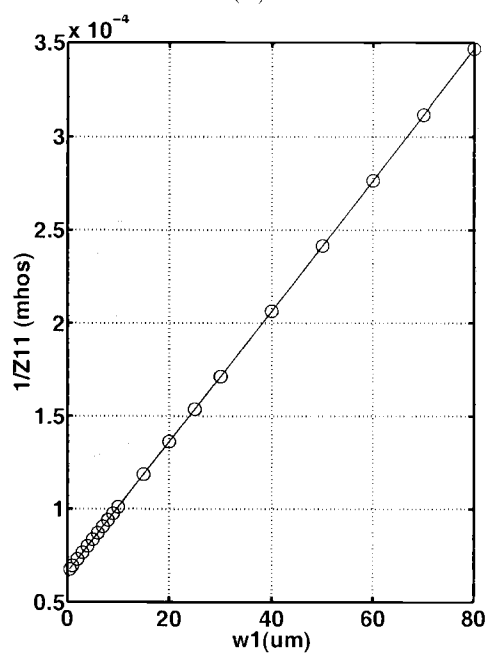
$$a = 6.5942 \times 10^{-5} \frac{1}{\Omega} \quad b = 3.5092 \frac{1}{\Omega m}$$

The plot of $1/Z_{11}$ in Fig. 3.8 (b) shows good agreement between the model of Eq.(3.2) and the data extracted from MEDICI simulations.

The next step in Z_{11} modeling is to understand the influence of two or more contacts on Z_{11} . The current flow lines for different separations provide insight into the relationship between Z_{11} and the contact locations. In Fig. 3.9 (a) a single contact is shown, while Figs. 3.9 (b), (c) and (d) illustrate two contacts with $5\mu m$, $10\mu m$ and $40\mu m$ separations, respectively. The injector contact size is chosen as $w_1 = 0.5\mu m$, and the sensor contact size is $w_2 = 10\mu m$. From these plots, it can be observed that for a single contact in Fig. 3.9 (a), all of the current flows from the contact to the backplane. For a $5\mu m$ separation in Fig. 3.9 (b), the current also flows to the backplane, but the second contact affects its distribution and hence the value of Z_{11} . Also for a separation of $10\mu m$ in Fig. 3.9 (c), all the current flows to the



(a)



(b)

Figure 3.8. (a) Z_{11} vs. contact width. (b) $1/Z_{11}$ vs. contact width and its fit to a line.

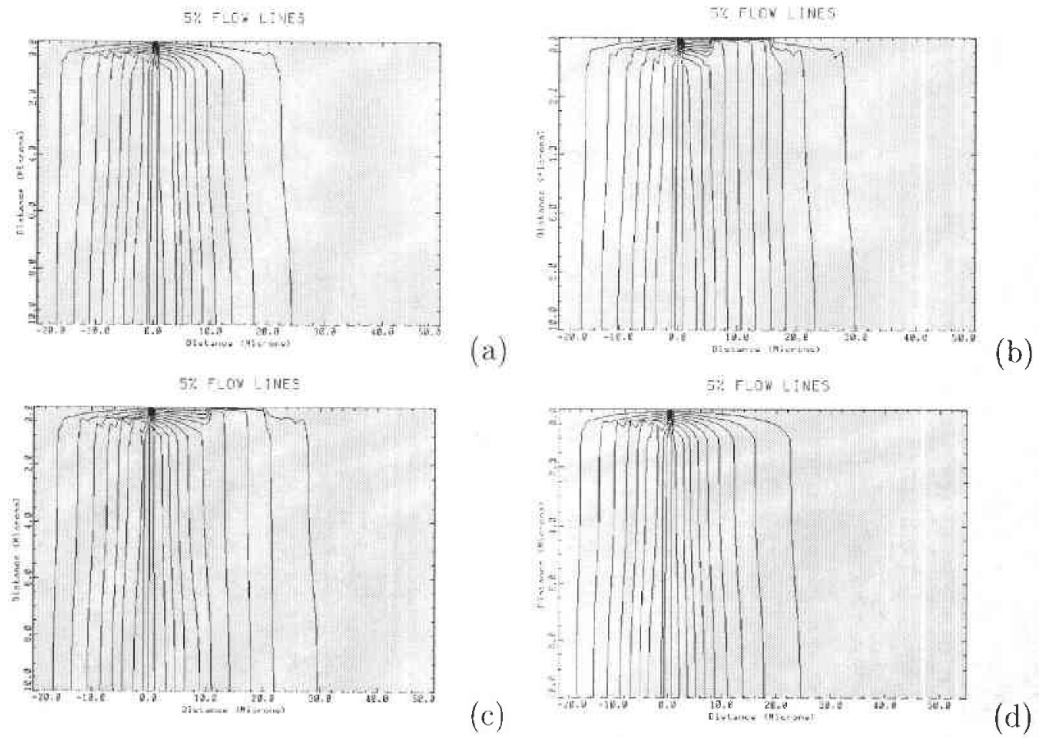


Figure 3.9. Current flow lines in a heavily doped substrate for:
 (a) Single contact case. $Z_{11} = 14.79K\Omega$.
 (b) $5\mu m$ separation between the source and sensor. $Z_{11} = 13.05K\Omega$.
 (c) $10\mu m$ separation between the source and sensor. $Z_{11} = 14.18K\Omega$.
 (d) $40\mu m$ separation between the source and sensor. $Z_{11} = 14.79K\Omega$.

backplane but the value of Z_{11} is different from the first two cases. In Fig. 3.9 (d), the current flow lines are found to be the same as in the single contact case. Thus it can be concluded that for separations larger than a certain value, the injector contact behaves as a single contact, and Z_{11} is not affected by the neighbouring contact. It is observed that for a $20\mu m$ separation Z_{11} is within 1% of its value for large separations, which is equal to $1/(a + bw_1)$, while it is within 10% of this value for a $10\mu m$ separation. For this reason, the above model for Z_{11} is valid only for separations larger than $10\mu m$.

The simulated values of Z_{12} show an exponentially decaying behavior as in Fig. 3.10. The model for separations larger than $10\mu m$ is obtained as:

$$Z_{12} = \alpha e^{-\beta x} \quad (3.3)$$

where α and β are process parameters obtained from curve fitting. From MEDICI simulations in Fig. 3.11 it can be seen that β is independent of contact widths.

The values obtained for the substrate profile used in this particular simulation are:

$$\alpha = 233 \ \Omega \quad \beta = 1.0666 \times 10^5 \ \frac{1}{m}$$

Next, the model is verified by comparing the values of the cross-coupling resistances obtained from the model with simulated values. The two-port Y parameters for the substrate macromodel are given by:

$$Y = \begin{bmatrix} y_{11} & y_{12} \\ y_{21} & y_{22} \end{bmatrix} = \frac{1}{|Z|} \begin{bmatrix} Z_{22} & -Z_{12} \\ -Z_{21} & Z_{11} \end{bmatrix} = \begin{bmatrix} G_{11} + G_{12} & -G_{12} \\ -G_{21} & G_{21} + G_{22} \end{bmatrix}$$

Therefore,

$$G_{12} = -y_{12} = \frac{Z_{12}}{|Z|}$$

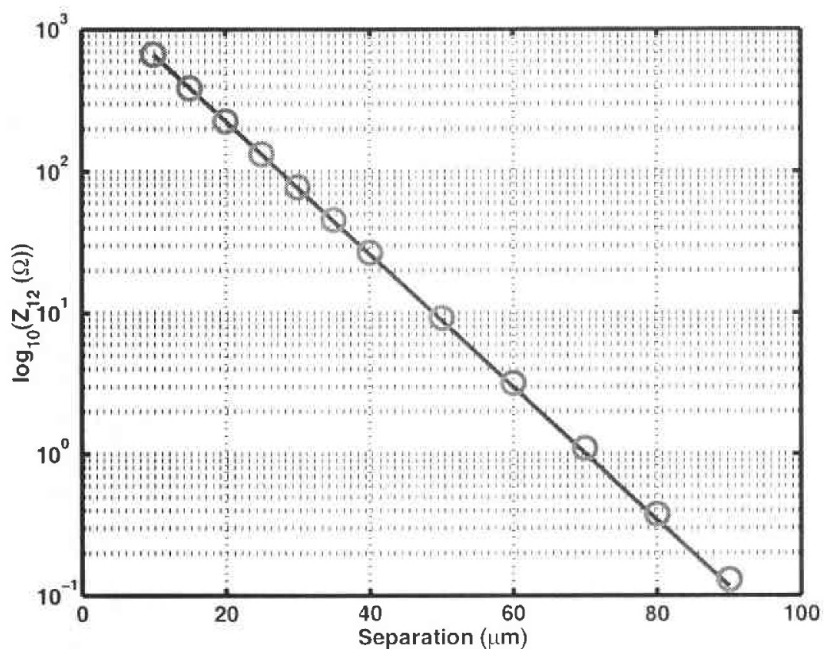


Figure 3.10. Logarithm of Z_{12} as a function of separation in heavily doped substrates. The two contacts are $5\mu\text{m}$ and $100\mu\text{m}$ wide.

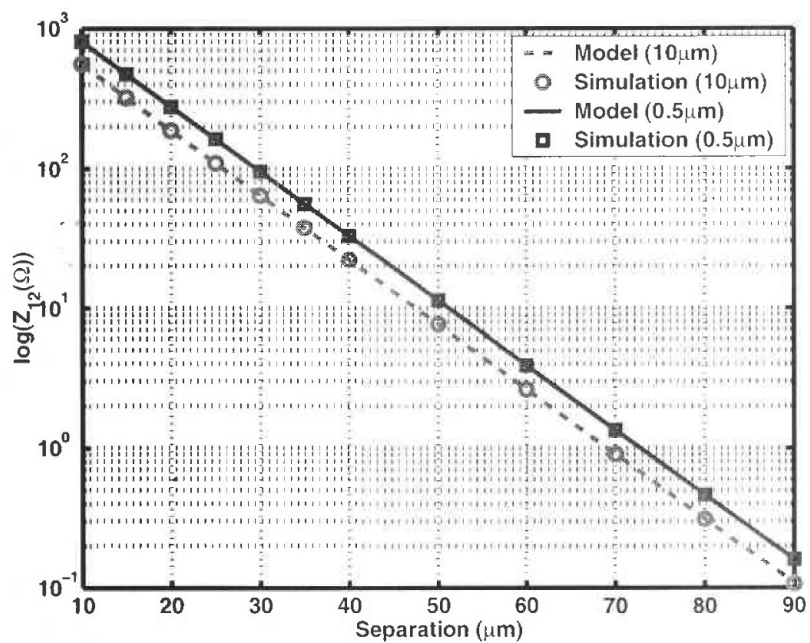


Figure 3.11. Medici simulations show that β is independent of contact widths. In this figure β is the slope of the $\log(Z_{12})$ curve.

which gives

$$R_{12} = \frac{|Z|}{Z_{12}} = \frac{|Z|}{Z_{21}}$$

where $|Z|$ is the determinant of the Z matrix. Y , Z , G and R matrices are symmetric because the resistive network between the contacts is a reciprocal one. The R_{12} values for different separations (x) and contact widths calculated from the Z parameters and obtained from MEDICI simulations are shown in Table 3.1.

<i>Source</i> (μm)	<i>Sensor</i> (μm)	R_{12} ($x = 10\mu m$)		R_{12} ($x = 40\mu m$)		R_{12} ($x = 100\mu m$)	
		Model	Sim.	Model	Sim.	Model	Sim.
0.5	0.5	39.2K Ω	38.7K Ω	1.08M Ω	1.04M Ω	659M Ω	591M Ω
0.5	5	40K Ω	38.6K Ω	1.08M Ω	1.04M Ω	651M Ω	590M Ω
0.5	100	43.1K Ω	38.6K Ω	1.08M Ω	1.04M Ω	649M Ω	590M Ω
2	5	40.2K Ω	38.5K Ω	1.08M Ω	1.04M Ω	649M Ω	589M Ω
5	5	40.6K Ω	38.5K Ω	1.08M Ω	1.04M Ω	647M Ω	588M Ω
10	100	41.9K Ω	38.5K Ω	1.04M Ω	1.04M Ω	628M Ω	588M Ω

Table 3.1. R_{12} values calculated from the Z -parameter-based model compared with the values obtained from MEDICI simulations.

A comparison of the data in Table 3.1 shows that the worst case error is 11.66% for a separation of $10\mu m$, while for $40\mu m$ and $100\mu m$ separations the errors are 3.8% and 11.5%, respectively. The calculated resistance values are in agreement with the values obtained from resistance based approach in [6].

3.4. Extension of the Model to the Third Dimension

Although 2D device simulations are useful to illustrate substrate coupling mechanisms, they cannot explain the influence of 3D geometries on substrate noise coupling. For a 2D simulator a user can only define the substrate profile, including thicknesses, doping levels and the contact widths in the input file. Hence, it is impossible to predict coupling for different contact shapes using 2D simulations. Fig. 3.12 illustrates 2D and 3D substrate structures. In a 2D structure only the contact widths are defined, contact lengths can also be defined in a 3D structure.

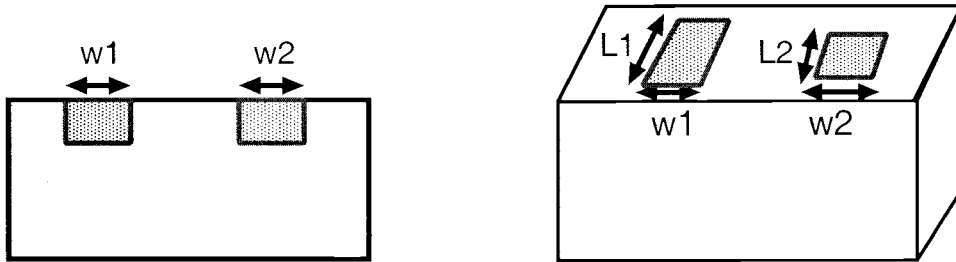


Figure 3.12. 2D and 3D cross sections of a substrate with two contacts.

To develop a model that is scalable with contact sizes and spacing, several simulations were performed for heavily and lightly doped substrates using Agilent/EEsof-Momentum [14], which is a 2.5-dimensional simulator assuming an infinite die area. Agilent/EEsof-Momentum is an electromagnetic simulator which allows the user to define different contact shapes in a layout, and produces an N -port S -parameter output file, where N is the number of contacts in the layout. From these S parameters, Z parameters can be calculated as described in Appendix A.

The key idea of the new macromodel is to enable calculation of multiple port resistance values using two-port Z parameters. Accordingly, most of the simulations were done using two contacts for a two-port model extraction. Multiple port simu-

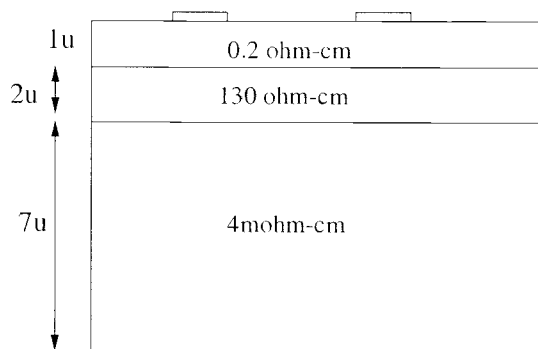


Figure 3.13. Substrate geometry for simulation of a heavily doped substrate in Momentum.

lations were done to understand the effect of nearby contacts on Z parameters. In order to verify simulation results obtained from Momentum, another 3D simulator EPIC was used [15]. EPIC is a program that extracts substrate resistances and capacitances using the Green's function method [2]. The substrate resistances are calculated for the doping profiles for the $0.5\mu m$ MOSIS HP CMOS process shown in Fig. 3.13. The calculated resistance values in this figure are average values for the $0.5\mu m$ MOSIS HP CMOS process, so they differ from the values for a general heavily doped substrate as shown in Fig. 3.6. An analysis of the data obtained from Momentum simulations shows that Z_{11} is a function of the contact area and the contact perimeter. Hence, Z_{11} can be expressed as:

$$Z_{11} = \frac{1}{K_1 \cdot Area + K_2 \cdot Perimeter + K_3} \quad (3.4)$$

where K_1 , K_2 and K_3 are empirical fitting parameters. This model for Z_{11} is an improvement over that proposed in [6] and is similar to the contact self-resistance model in [12].

For a square contact, $1/Z_{11}$ increases quadratically with the contact width as shown in Fig. 3.14. It is seen that the model accurately predicts the simula-

tion results. The measured data from [6] is also used to verify the Z_{11} model. In

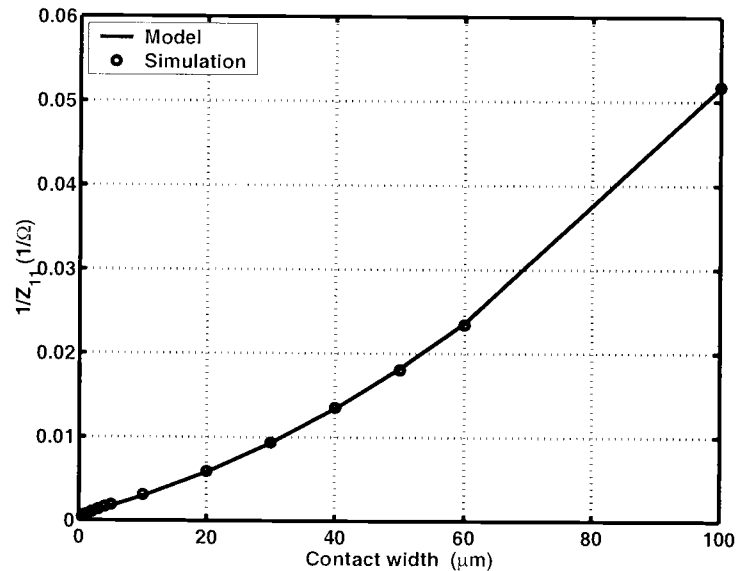


Figure 3.14. $1/Z_{11}$ versus width for square contacts comparing the model and simulations.

Fig. 3.15, the model is compared with measured data and simulations and one can see that there is good agreement between them. The deviations of the measured and simulated Z_{11} values are expected due to the uncertainty in the substrate doping profiles used in simulations.

The Z_{11} dependence on nearby contacts is also examined for 3D geometries. Momentum simulation results show that for separations larger than $10\mu\text{m}$, Z_{11} values do not change due to nearby contacts. Fig. 3.16 summarizes the simulation results for $5\mu\text{m} \times 5\mu\text{m}$ contacts. The first part of this figure shows a single contact with a simulated Z_{11} value of 535Ω . When this single contact is surrounded by four identical contacts at a separation of $0.5\mu\text{m}$, the value of Z_{11} drops to 403Ω due to the nearby contacts. When the separation from the surrounding contacts increases to $10\mu\text{m}$, Z_{11} becomes 528Ω as shown in the third part of Fig. 3.16. For separations larger than $10\mu\text{m}$, Z_{11} converges to a single contact value. Fig. 3.16 shows that

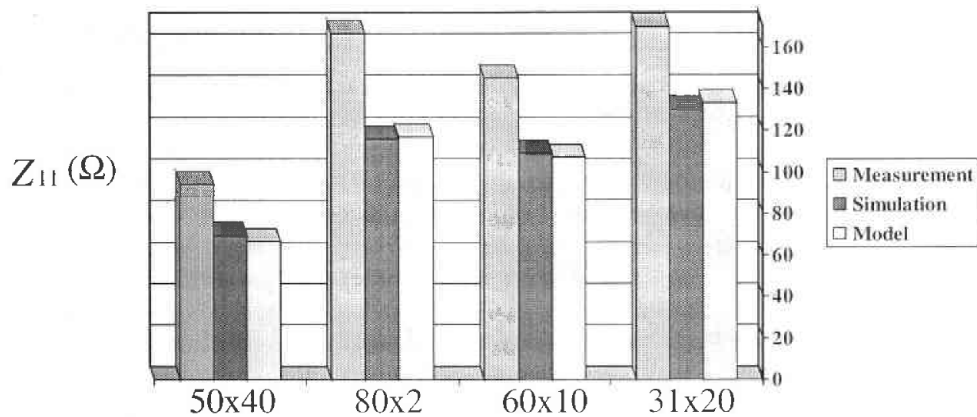


Figure 3.15. The Z_{11} model is in good agreement with measurements from [6] and Momentum simulations.

the open circuit parameters stay constant for separations larger than $10\mu m$. The parameter extraction process for Z_{11} is summarized in Appendix B.

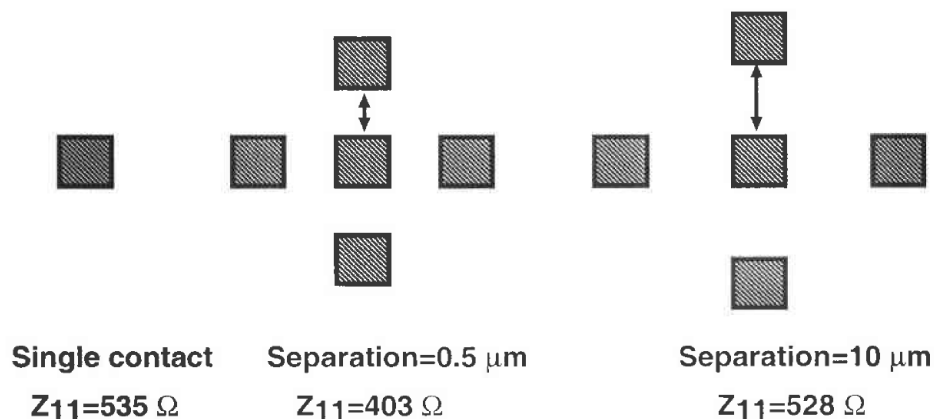


Figure 3.16. 3D simulation results showing Z_{11} dependence on nearby contacts.

On the other hand Z_{12} , is a function of the contact geometries and the spacing. The simulated values of Z_{12} have an exponentially decaying behavior with increasing separation between the contacts as shown in Fig. 3.17. From this observation, Z_{12} is modeled as:

$$Z_{12} = \alpha e^{-\beta x} \quad (3.5)$$

where β is a process dependent parameter, and α is the value of Z_{12} , at $x = 0$. Z_{12} values were obtained for a separation larger than $10\mu m$, which is the minimum distance for which the model is applicable. The value of α has a dependence on contact dimensions as does Z_{11} . At zero separation the two contacts merge into a single contact and the value of α is equal to the Z_{11} value of this single merged contact. Therefore the value of α can be calculated by using the total area and perimeter of the merged contact.

In this model, α introduces the area and perimeter dependence of contacts in the Z_{12} model, whereby the contact cross-coupling resistances depend on area, perimeter and spacing of contacts. This is a significant difference from the model of [12] where the perimeter dependence is completely ignored for the cross-coupling resistances.

From simulations it is also observed that β is independent of the contact dimensions and is a constant for a given process. For this reason, the value of β can be obtained by curve-fitting simulated or measured data. A comparison of the model and simulations for Z_{12} is shown in Fig. 3.17 and good agreement between the model of (3.5) and simulations is obtained. From this figure, it can also be seen that β is independent of the contact geometry since the slopes of $\log(Z_{12})$ for different contact sizes are identical. The parameter extraction process for Z_{12} as a function of x is summarized in Appendix C.

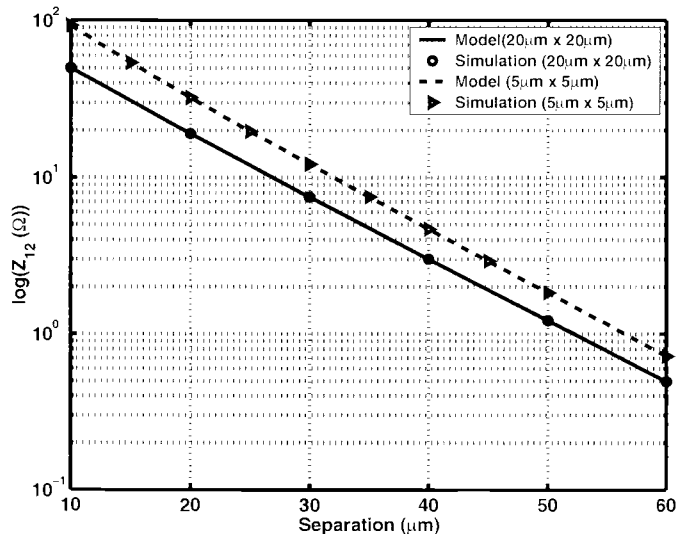


Figure 3.17. Simulations and model for Z_{12} show that β is independent of contact sizes. The model and simulations are in good agreement.

3.5. Model for Contacts with Different Sizes

So far only rectangular contacts with identical sizes in the third dimension have been considered. This is not the case in an actual layout as shown in Fig. 3.18. In this section, the modeling of different contact shapes and their relative positioning in heavily doped substrates is addressed. The relative positions of two contacts is important when one of the contacts is smaller than the other one. An example of two contacts with different sizes is shown in Fig. 3.18. The separation x is the distance between the inner edges of the two contacts. The relative position, y , is defined to be zero when the bottom edges of two contacts are aligned and increases in the direction of the arrow, as shown in Fig. 3.18.

According to the proposed Z -parameter model, Z_{12} between two contacts decreases exponentially with an increase in the separation x as illustrated in Fig. 3.19, where both contacts are assumed to have the same length in the y direction.

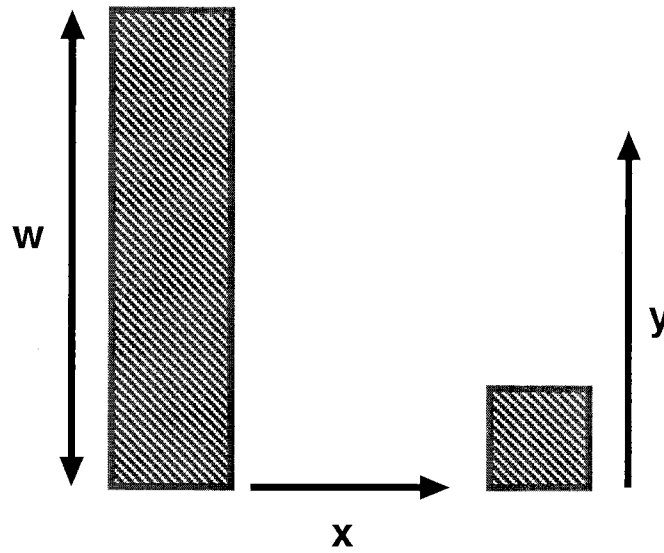


Figure 3.18. Two contacts with different sizes.

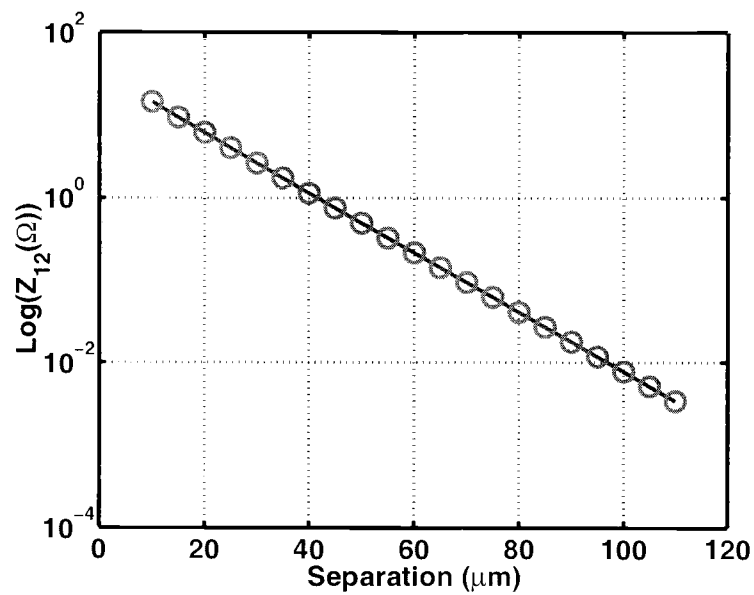


Figure 3.19. Simulations and model for Z_{12} show that Z_{12} decays exponentially with increasing separation (x) between the contacts.

Fig. 3.20 shows the dependence of Z_{12} on different y values, for a fixed separation $x = x_a$. Z_{12} is a maximum when the center of the small contact coincides with the center of the large one. In Fig. 3.18, the maximum coupling occurs when the center of the small contact coincides with $w/2$.

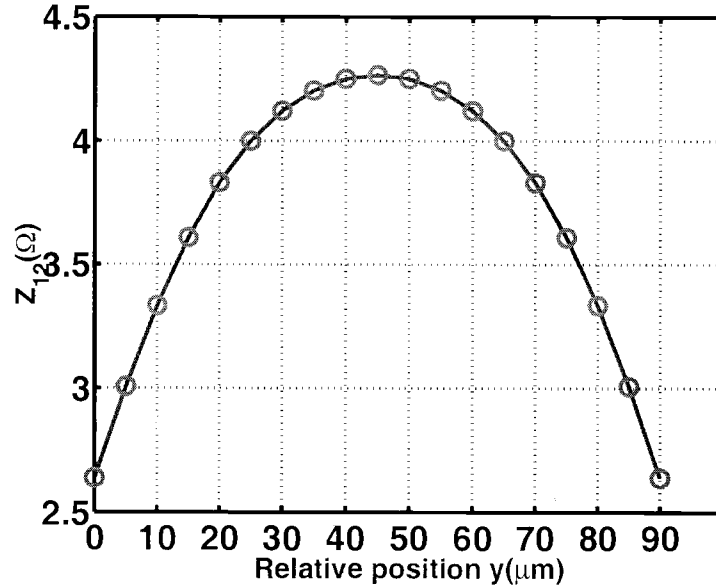


Figure 3.20. Simulations for $w = 100\mu\text{m}$ show that Z_{12} has a quadratic dependence on y when $x_0 = 35\mu\text{m}$. The maximum value of Z_{12} is at $y = 45\mu\text{m}$.

A curve fit on the data of Fig. 3.20 shows that Z_{12} can be modeled as a polynomial function of y .

$$Z_{12} = ay^2 + by + c \quad (3.6)$$

The coefficients a and b are related to each other since Z_{12} is symmetrical with $w/2$.

Therefore,

$$\frac{w}{2} = \frac{-b}{2a} \quad (3.7)$$

whereas c is equal to the value of Z_{12} at a separation $x = x_a$.

$$c = Z_{12}|_{x=x_0} = \alpha e^{-\beta x_0} \quad (3.8)$$

In (3.8), x_a is the separation used for curve fitting the y dependence of Z_{12} . Hence, only one additional parameter is required to model the Z_{12} dependence on the relative contact position.

The coefficients a , b and c are scalable with contact dimensions. Therefore once the parameters are extracted for a specific geometry, they can be scaled for different contact geometries. Fig. 3.21 shows two contacts at $x_0 = 0$ for three different values of y . For these three different cases, the maximum deviation in the simulated value of Z_{11} is 1.6 %.

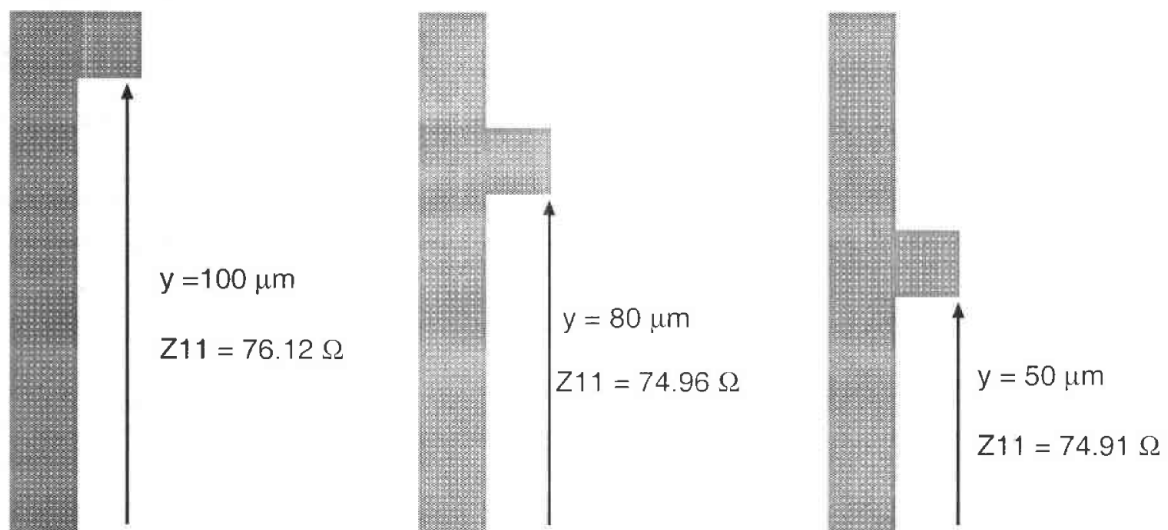


Figure 3.21. A large ($10\mu\text{m} \times 110\mu\text{m}$) and small ($10\mu\text{m} \times 10\mu\text{m}$) contact for three different relative positions. The value of Z_{11} is constant for a fixed area and perimeter. Since the Z_{11} (α) value is independent of y , parameters a , b and c are scalable with contact dimensions.

This example shows that parameters a , b and c have the same dependence on contact dimensions. Therefore, the parameters can be scaled for different geometries using

$$a_{new} = a_{old} \times \frac{\alpha_{new}}{\alpha} \quad b_{new} = b_{old} \times \frac{\alpha_{new}}{\alpha} \quad c_{new} = c_{old} \times \frac{\alpha_{new}}{\alpha} \quad (3.9)$$

where α and α_{new} are equal to the Z_{11} value of the merged contacts before and after scaling, respectively. In Fig. 3.21, the length of the second contact is very small with respect to the first one. Two equal-sized contacts for two different y positions are shown in Fig. 3.22. Simulated Z_{11} values are again constant for $y = 0\mu m$ and $y = 50\mu m$ with a deviation of 3.3 % in the Z_{11} value. This example verifies that the parameters a , b and c are scalable with contact dimensions.

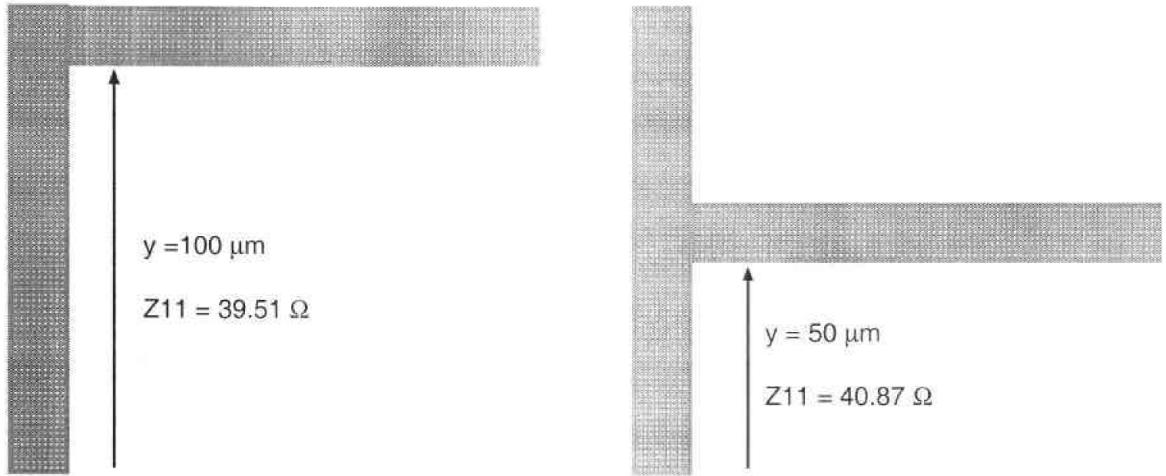


Figure 3.22. two contacts of size $(10\mu m \times 110\mu m)$ and $(110\mu m \times 10\mu m)$ for two different relative positions at zero separation ($x = 0$). The value of Z_{11} is constant for a fixed area and perimeter. This example verifies that the parameters a , b and c are scalable with contact dimensions.

The parameter extraction process for Z_{12} as a function of y is summarized in Appendix C.

When x and y change at the same time, Z_{12} can be modeled as the product of these two effects.

$$Z_{12} = [ay^2 + by + c] e^{-\beta(x-x_a)} \quad (3.10)$$

Fig. 3.23 shows good agreement between expression (3.10) and simulation results when x and y change concurrently.

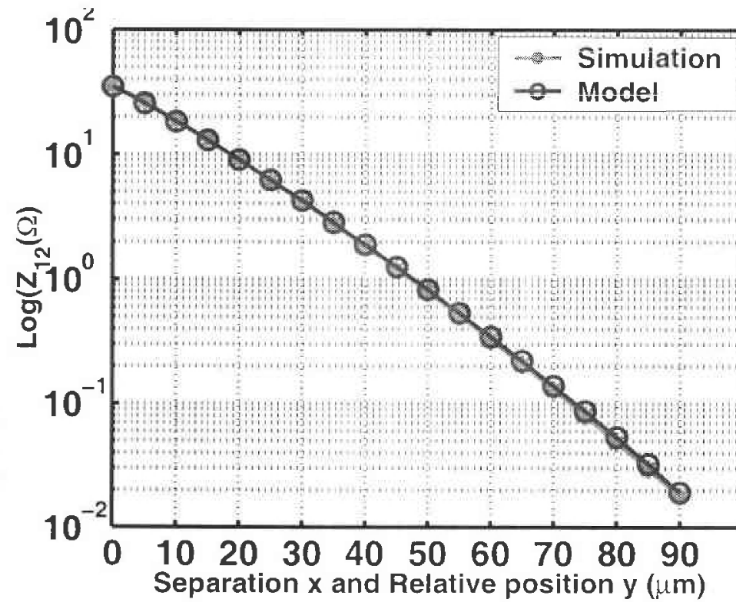


Figure 3.23. Model predicts the simulation results for Z_{12} for variations in x and y .

When one contact is surrounded by another contact as shown in Fig. 3.24, the number of interacting (coupling) sides is more than one. In such cases, the first step in the Z_{12} calculation is to divide the complex contact shape into rectangular contacts. Then the coupling between each rectangular part and the contact that they surround are calculated separately. Finally, the overall Z_{12} between the two contacts is the superposition of the calculated Z_{12} values. Fig. 3.24 illustrates two sided coupling between an L-shaped and a square contact. In this example the L-shaped contact is divided into two rectangular contacts 1 and 2. Z_{12} is calculated as a superposition of couplings from these two contacts to the small one.

The model predicts simulated Z_{12} values for different y as shown in Fig. 3.25 for the contact geometries of Fig. 3.24.

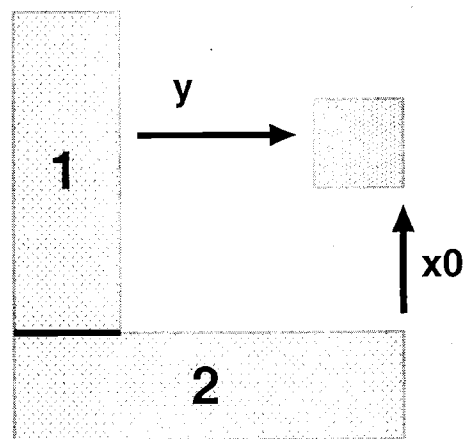
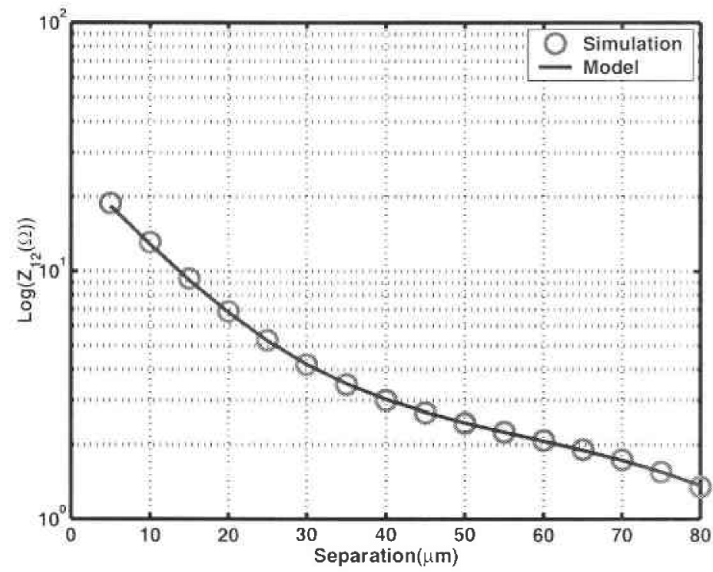
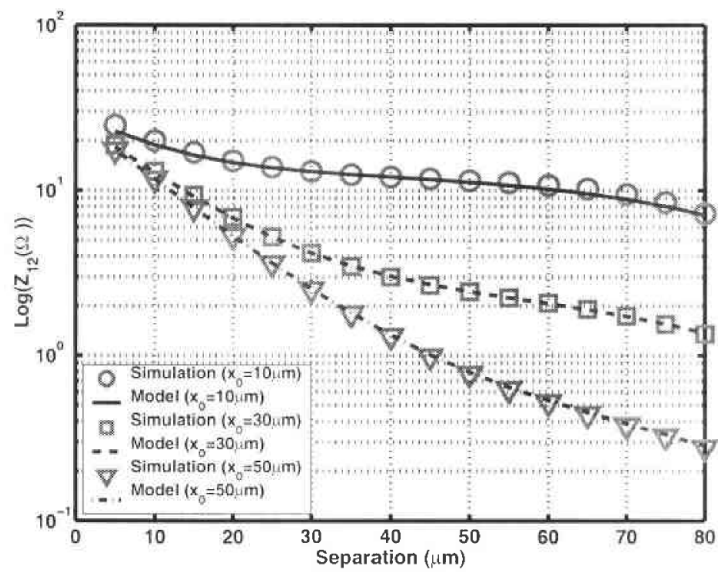


Figure 3.24. An example of an L-shape and square contact illustrating two sided coupling.



(a)

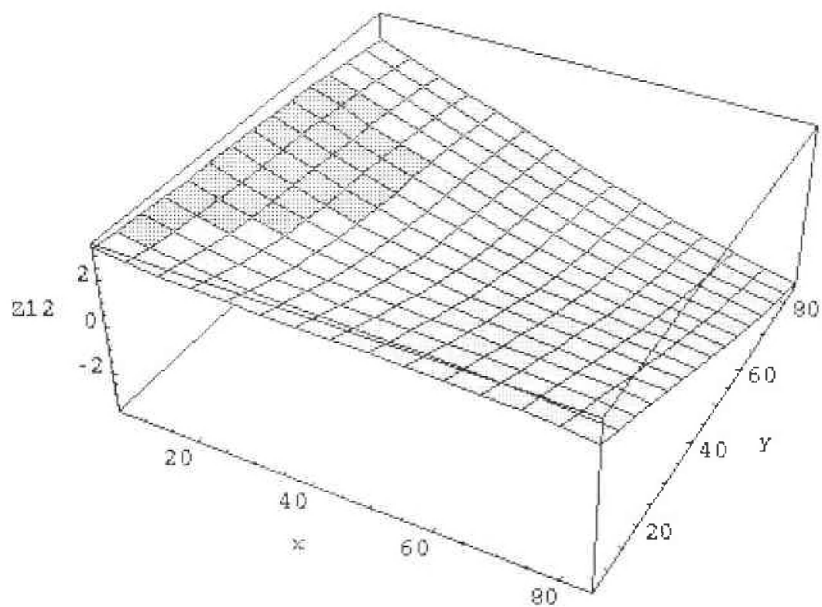


(b)

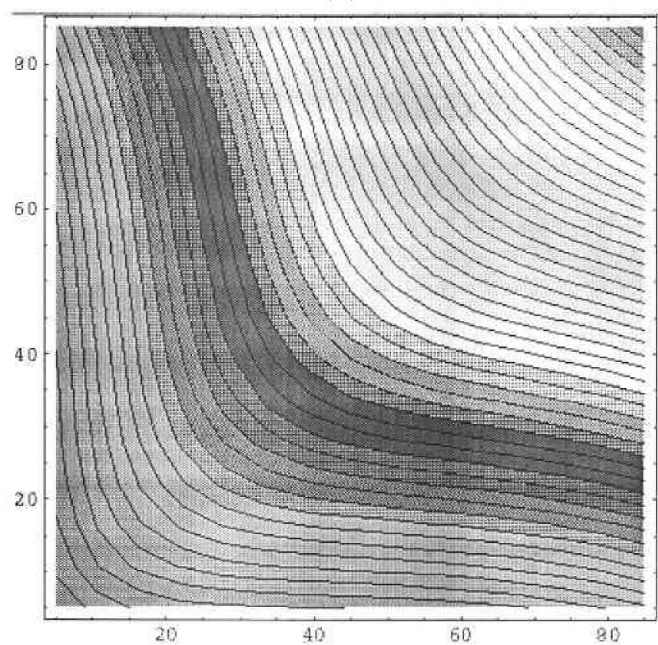
Figure 3.25. The model and simulations are in agreement for the contacts in Fig. 3.24 for (a) $x_0 = 30\mu\text{m}$, (b) different x_0 values. The L-shaped contact consists of two $10\mu\text{m} \times 100\mu\text{m}$ rectangles and the square contact is $10\mu\text{m} \times 10\mu\text{m}$.

Each of the curves in Fig. 3.25 is a cross section of a 3D Z_{12} plot as a function of x and y , from Fig. 3.26. Consider the movement of the small square contact along the contour lines shown in Fig. 3.26 (b). When the small contact is close to section 1 of the L-shaped contact, the major coupling component will be due to section 1. This situation is illustrated as point A in Fig. 3.27. Whereas, when the small contact is at point B, the maximum coupling is due to section 2. At C, the contact is equidistant from both the sections, hence the coupling from both sections is equally significant. Because of the coupling from both sections, the Z_{12} value is the same as that of A or B, even though it is not at a minimum distance from any section. Note that there is a symmetry axis along the diagonal of the L shape due to the symmetry of contact shape, and the constant Z contours are symmetric with respect to this axis. The proposed model was also tested on asymmetric shapes and a good agreement between the model and simulations has been obtained as shown in Fig.3.28.

Fig. 3.29(a) illustrates an example of three sided coupling between a U-shaped and a square contact. The model predicts the simulated values accurately, as shown in Fig. 3.30. Fig. 3.30 (a) shows a comparison of the model and the simulated Z_{12} values for varying y at five different separations x_0 . The comparison of the Z_{12} values for varying x and fixed y is shown in Fig. 3.30 (b). The model is also verified for a four sided coupling example shown in Fig. 3.29(b). Fig. 3.31 illustrates the model versus simulation results for this example. Matlab codes for model parameter extraction for Z_{11} and Z_{12} are also provided in Appendices B and C respectively.



(a)



(b)

Figure 3.26. 3D Z_{12} plot and the constant Z_{12} contour lines show the coupling between the contacts in Fig. 3.24: (a) 3D Z_{12} plot. (b) Constant Z_{12} contours.

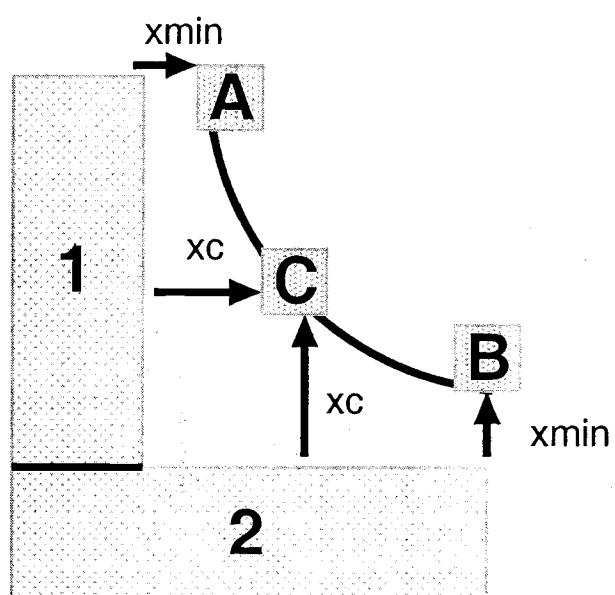
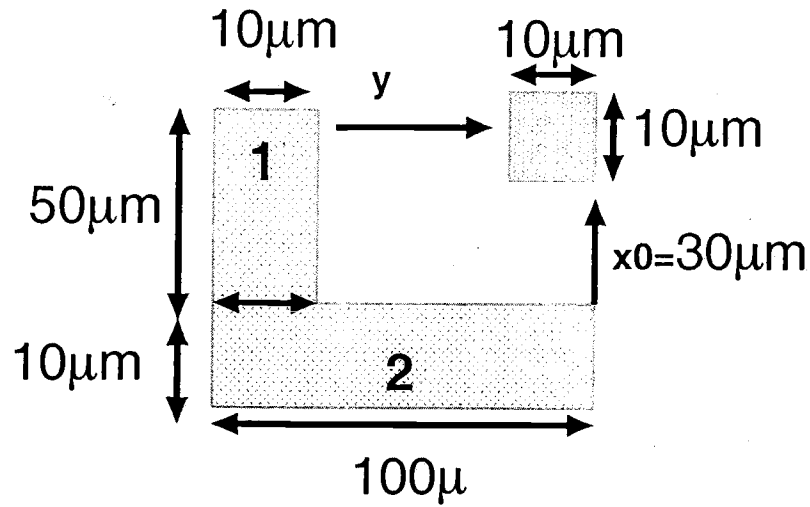
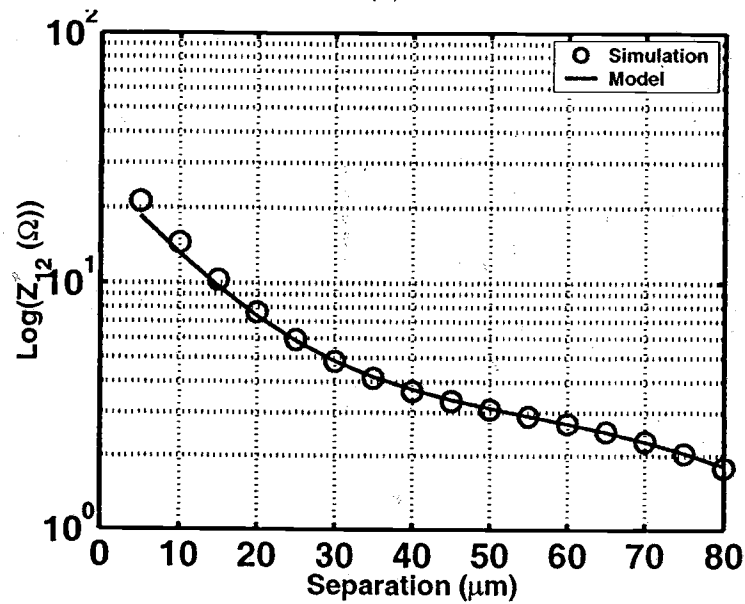


Figure 3.27. Illustration of the movement of the small contact along one of the contour lines shown in Fig. 3.26 (b).

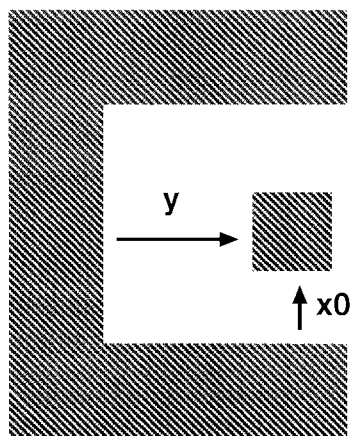


(a)

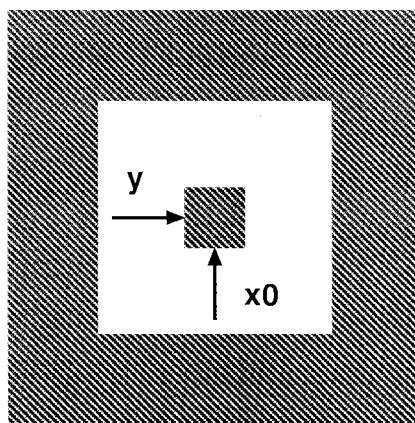


(b)

Figure 3.28. The model also works for asymmetric geometries. (a) An asymmetric L-shaped contact and a square contact. (b) Model agrees with the simulation results for different y values for the contact geometries of (a) with a maximum error of 12.6%.

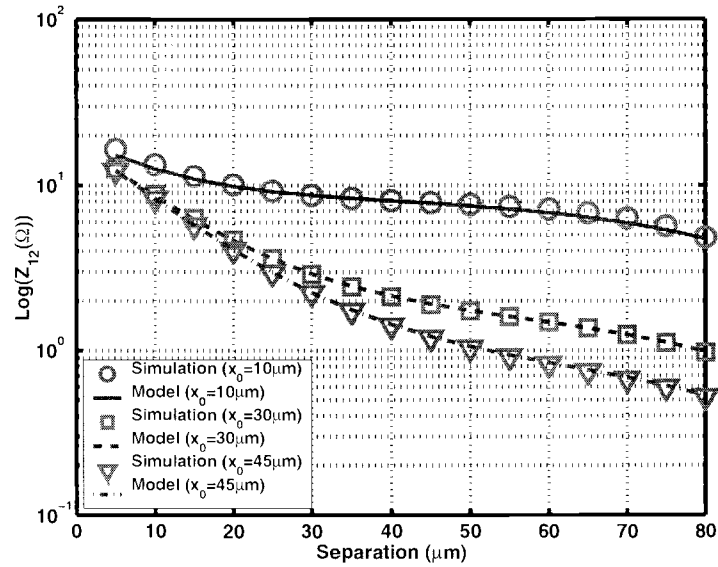


(a)

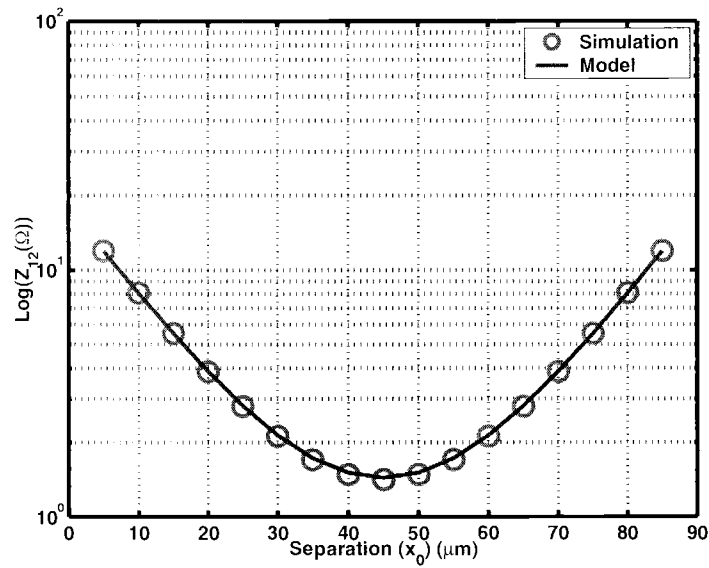


(b)

Figure 3.29. (a) A U-shaped and a square contact. (b) The square contact is completely surrounded by another contact.

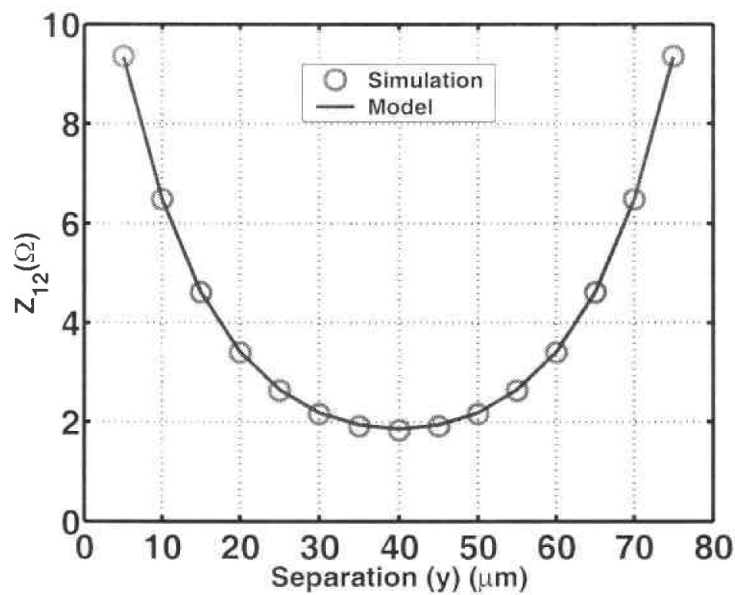


(a)

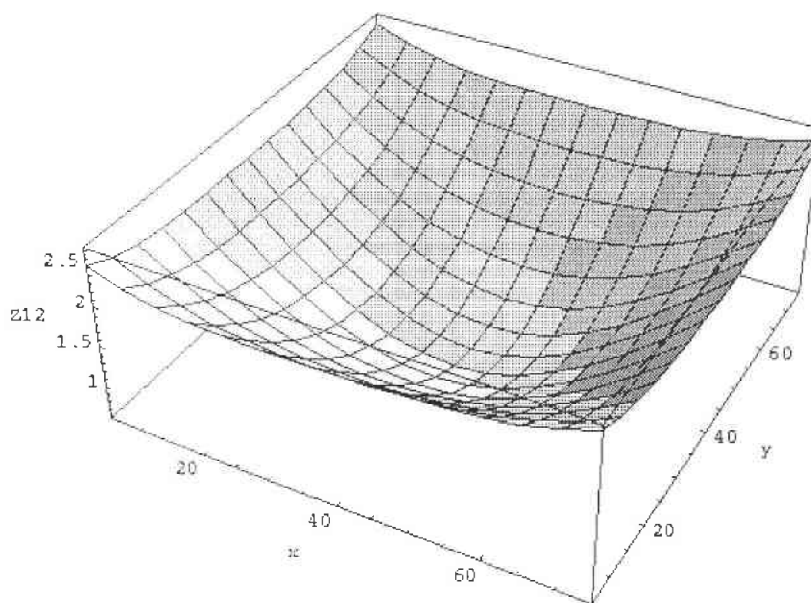


(b)

Figure 3.30. The model and simulations agree for the contact geometry in Fig. 3.29 (a). (a) Logarithm of Z_{12} versus y for three different x_0 values obtained by using the model. (b) Logarithm of Z_{12} versus x_0 when $y = 40\mu\text{m}$. In this example the U-shaped contact consists of three rectangular contacts of size $100\mu\text{m} \times 10\mu\text{m}$, and the square contact is $10\mu\text{m} \times 10\mu\text{m}$.



(a)



(b)

Figure 3.31. (a) The model agrees with simulations for the contacts shown in Fig. 3.29 (b) when $x_0 = 40\mu\text{m}$. (b) 3D plot of Z_{12} shows that the minimum value of Z_{12} occurs in the middle of the surrounding contact. The square contact consists of four rectangular contacts of size $100\mu\text{m} \times 10\mu\text{m}$, where the square contact is $10\mu\text{m} \times 10\mu\text{m}$.

4. PRELIMINARY MODEL FOR LIGHTLY DOPED CMOS SUBSTRATES

4.1. 2D Simulations in Lightly Doped Substrates

A substrate thickness of $20\mu\text{m}$ was used instead of $675\mu\text{m}$ specified by the process information in MEDICI simulations. This was done since only a limited number of grid points can be used in MEDICI.

MEDICI simulations for lightly doped substrates show that Z_{11} is constant for different contact widths. The p+ channel-stop implant layer in a lightly doped substrate creates a low resistance path for current to flow. Therefore, the injected current first spreads over the surface before it flows to the grounded backplane. In this type of substrate, the resistive path from the contact to the backplane is dependent on the overall chip surface, instead of just the contact dimensions. In Fig. 4.1 (a), the current flow lines indicate that the p+ channel-stop implant layer causes current spreading on the surface. For a homogeneous lightly doped substrate, the current does not spread on the surface as shown in Fig. 4.1 (b), and therefore Z_{11} changes with width.

The data extracted from MEDICI simulations is used to plot Z_{11} as a function of the contact width in Fig 4.2. Z_{11} stays constant with contact width as expected since a channel-stop implant layer was used in simulations.

Fig. 4.3 shows that the logarithm of Z_{12} decreases linearly with the separation, x . This linear behavior indicates that Z_{12} in lightly doped substrates decreases exponentially with the separation as it does in heavily doped substrates.

The curve of Fig. 4.3 can be represented as an exponential function of the separation. A curve fit on the data shows that Z_{12} in lightly doped substrates can be modeled as:

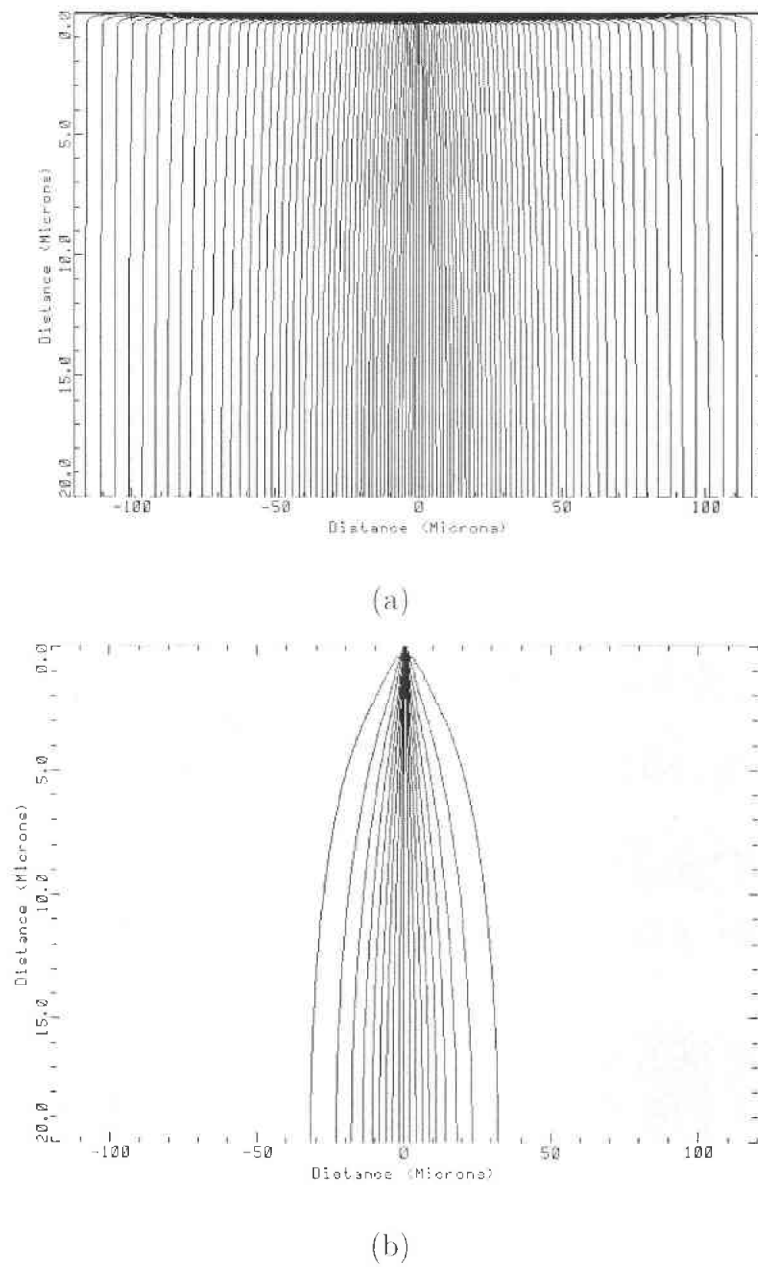


Figure 4.1. Current flow lines in a lightly doped substrate for a point contact in: (a) substrate with a channel-stop implant layer and (b) a homogeneous substrate.

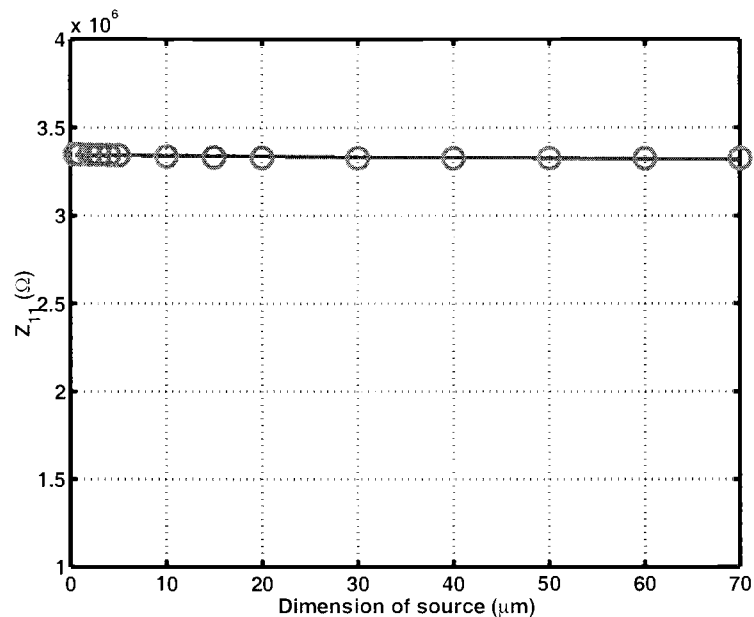


Figure 4.2. Z_{11} as a function of contact width.

$$Z_{12}(x) = \alpha e^{-\beta x} \quad (4.1)$$

where α and β are process dependent parameters that can be extracted from either device simulations or measurements. The model shows good agreement with MEDICI simulations as illustrated in Fig. 4.3. This figure also illustrates that the value of Z_{12} changes at a small rate with separation. The β value, for lightly doped substrates is considerably smaller than that for a heavily doped substrate.

4.2. Lightly Doped Substrate Modeling in 3D

As mentioned in section 4.1, the p+ channel-stop implant layer in lightly doped CMOS processes causes current spreading on the chip surface. Consequently, Z_{11} is also a function of the chip area in lightly doped substrates. Discontinuities in

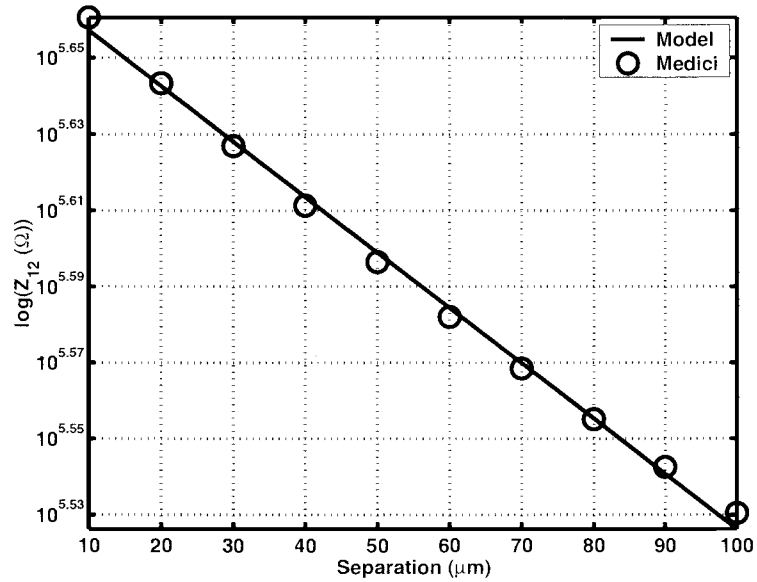


Figure 4.3. Logarithm of Z_{12} as a function of separation between the injecting and sensing contacts in a lightly doped substrate.

the channel-stop implant layer due to n-well structures would prevent the current flow on the chip surface. Hence the effective chip area for a contact will be smaller than the overall chip area. Fig. 4.4 shows the simulated dependence of Z_{11} on die area when the contact size is kept constant at $50\mu\text{m} \times 50\mu\text{m}$. For the same contact size Z_{11} is not a function of die area in heavily doped substrates as shown in Fig. 4.5. Simulation results were obtained by using EPIC. Similar results were obtained Cadence's tool SCA [16].

One of the shortcomings of a 2D device simulator such as MEDICI is that only the width of the contacts is taken into account during simulations. For a given contact width, the 3^{rd} dimension is assumed to be infinitely long. For heavily doped substrates the chip area does not introduce significant error as seen in Fig. 4.5.

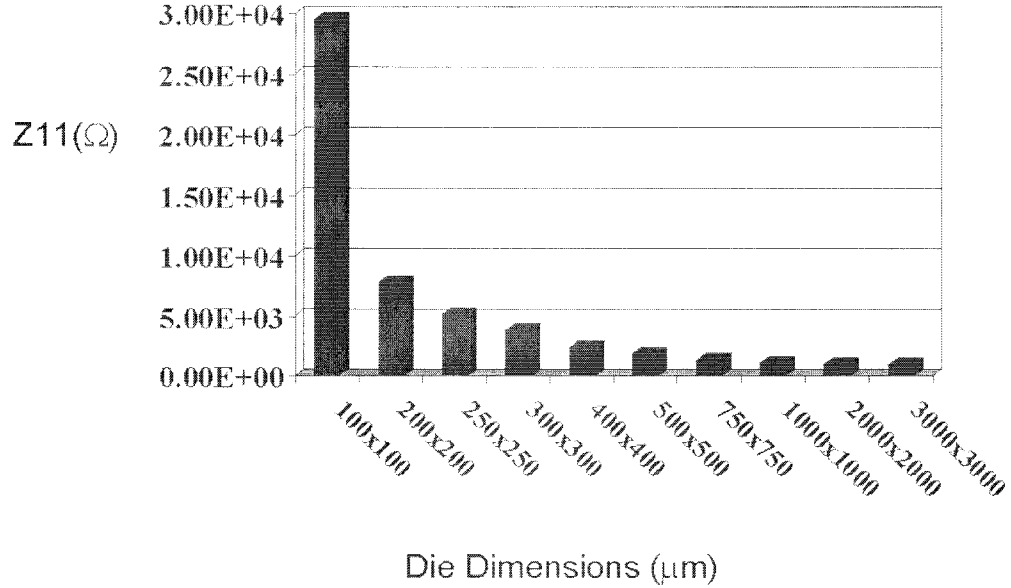


Figure 4.4. Simulations show that Z_{11} has a strong dependence on die area for a given contact size in lightly doped CMOS processes.

However, in a lightly doped substrate a significant difference is seen. In order to see the effect of contact dimensions it is a necessary to simulate lightly doped substrates using a 3D simulator. Fig. 4.6 illustrates that Z_{11} has a dependence on contact size for a constant die area according to Cadence SCA. EPIC simulation results support the same dependence as shown in Fig. 4.7.

A curve fit to SCA simulations results shows that Z_{11} in a lightly doped substrate can be modeled as:

$$Z_{11} = \frac{1}{K_1 \text{Perimeter} + K_2} \quad (4.2)$$

The model in (4.2) needs to be verified with other simulation tools. Die area and contact area dependence of Z_{11} should also be incorporated into the Z_{11} model. Momentum assumes an infinite die area for its simulations, making the tool un-

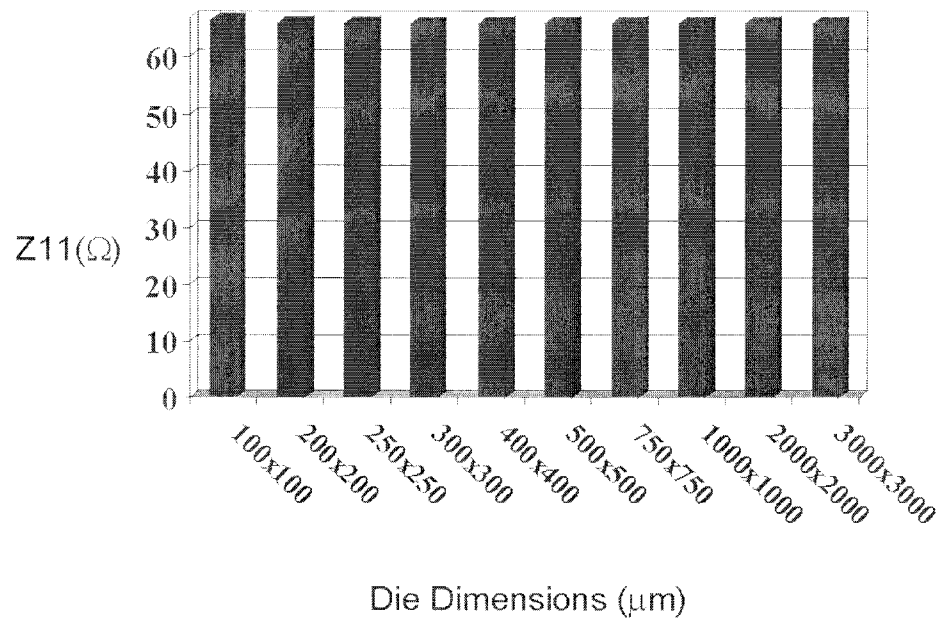


Figure 4.5. Z_{11} does not depend on die area for a given contact size in heavily doped CMOS processes.

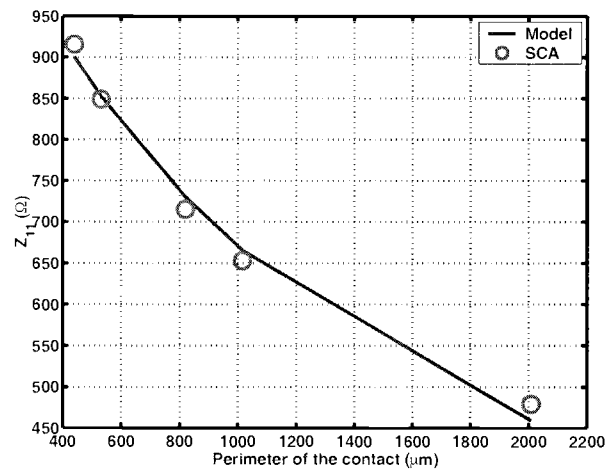


Figure 4.6. Simulations show that Z_{11} depends on contact size for a constant die area of $(1.2\text{mm} \times 0.24\mu\text{m})$. This result cannot be predicted by 2D device simulations.

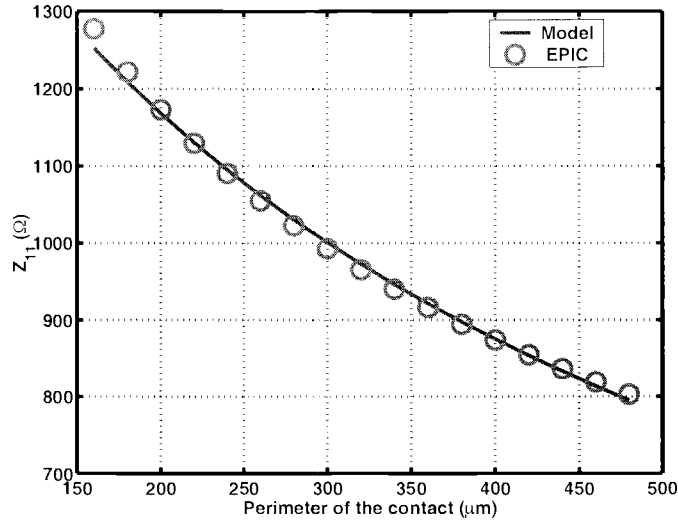


Figure 4.7. Z_{11} is a function of contact size for a constant die area of ($1\text{mm} \times 1\text{mm}$). EPIC simulation results agree with the SCA simulations.

suitable for simulations of lightly doped substrates. Limited availability of accurate simulation tools, and lack of experimental data for lightly doped substrates makes it difficult to model Z_{11} accurately for lightly doped substrates.

Simulation results for Z_{12} also show a behavior different from the MEDICI results in lightly doped substrates. Fig. 4.8 shows the logarithm of Z_{12} obtained from 3D EPIC simulations. This figure indicates that Z_{12} has to be modeled such that $\log(Z_{12})$ is linear for large separations and has a large value at zero separation. A 0th order modified Bessel function of second kind, $K_0(x)$, meets the above requirements for large separations. The leading term in the asymptotic expansion of $K_0(x)$ for large x is

$$\sqrt{\frac{\pi}{2x}} e^{-x} \quad (4.3)$$

The logarithm of (4.3) is equal to

$$\log(K_0(x)) = -x + \log\left(\sqrt{\frac{\pi}{2}}\right) - \frac{1}{2} \log(x) \quad (4.4)$$

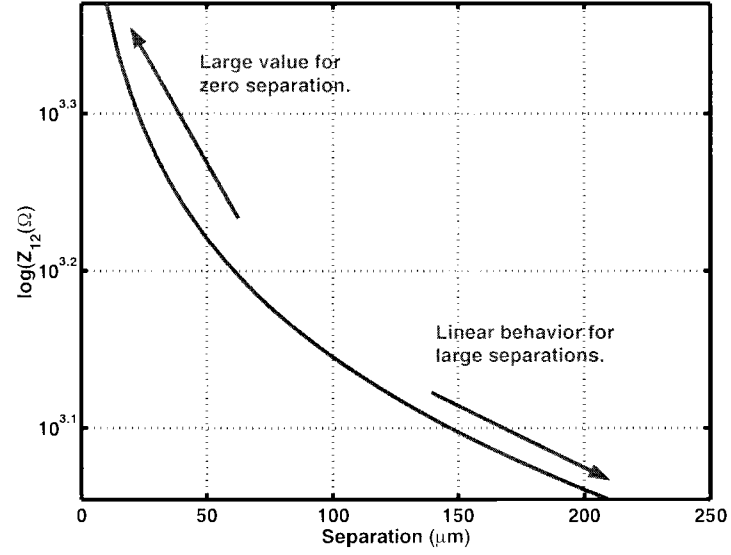


Figure 4.8. Logarithm of Z_{12} in lightly doped substrates. 3D simulation results are obtained from EPIC.

For large x

$$\frac{\log(x)}{x} \ll 1 \quad (4.5)$$

Hence, $\log(x)$ can be neglected with respect to x and $\log(\sqrt{\frac{\pi}{2}})$ is a constant term, in (4.3). Therefore logarithm of $K_0(x)$ changes linearly with the separation for large separations. Based on these observations Z_{12} in lightly doped substrates can be modeled as:

$$Z_{12}(x) = \alpha K_0(\beta x) \quad (4.6)$$

where α and β are process dependent parameters that can be extracted from either device simulations or measurements. The model shows good agreement with EPIC simulations as illustrated in Figure 4.9.

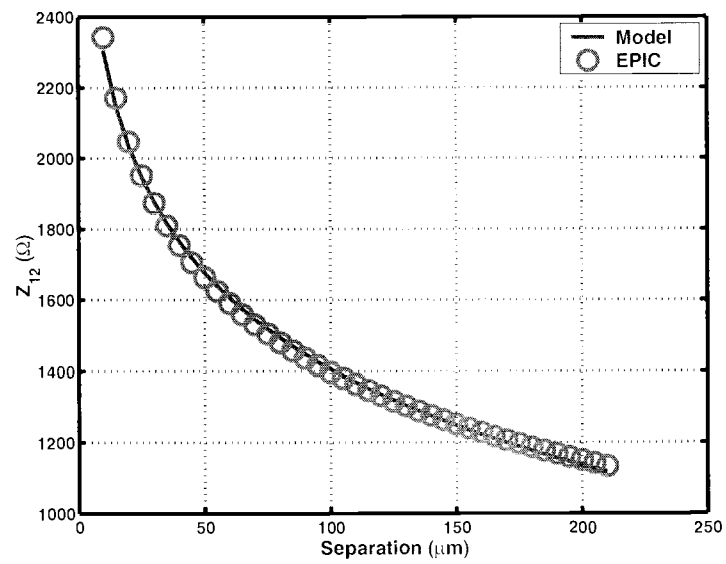


Figure 4.9. Simulations show that Z_{12} can be modeled as a modified Bessel function of the 0^{th} order. Model and the simulations are in good agreement. In this example the contacts are $2\mu\text{m} \times 2\mu\text{m}$ and the chip area is $(1\text{mm} \times 0.25\text{mm})$.

5. APPLICATION EXAMPLES AND COMPUTATIONAL EFFICIENCY

In the previous section, a scalable Z -parameter-based model has been developed for substrate resistance extraction. In this section, a comparison of the accuracy of the scalable model with simulations for a wide variety of contact shapes and spacings is given. These examples demonstrate that the model is both accurate and efficient in predicting substrate resistances.

The reason this approach is efficient is due to the scalability of the model with contact size. In other approaches, the contacts have to be divided into smaller panels and a large resistive network is extracted. In panel based approaches charge or current distribution is calculated for equipotential contact surfaces. Since the current distribution is not uniform on the surface, each contact needs to be divided into panels. As a result, the resistive array becomes very large and requires significant computational effort. The scalable model can be directly used to generate a compact network representation in an efficient manner. A simple example is illustrated in Fig. 5.1 where two contacts are shown and each contact is discretized into panels in existing non-scalable approaches. The simulated and calculated resistance values in Fig. 5.1 are compared in Table 5.1. The resistance values calculated from the scalable model are approximately the same as those from simulations. The error is less than 5%.

The scalable model can also be used for contacts of different shapes as shown in Fig. 5.2. The computed resistance values are shown in Table 5.2. Once again, the macromodel accurately computes the substrate resistances. All the resistance values are within 5% of the simulated values.

An example of three contacts is shown in Fig. 5.3. The resistance values for this example are presented in Table 5.3. In this case also, there is good agreement

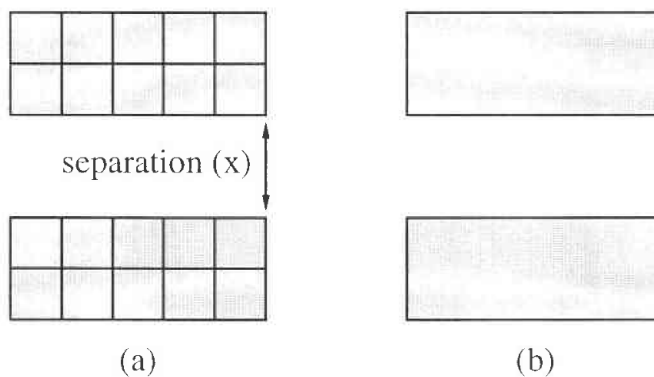


Figure 5.1. Calculation of substrate resistance networks comparing the conventional and the scalable modeling approaches. (a) Two large contacts are discretized into panels and the calculated cross-coupling resistance value for a separation of $40\mu\text{m}$ is $22.2\text{K}\Omega$. (b) For the scalable model the contacts are not discretized into panels. The calculated resistance value is $21.7\text{K}\Omega$.

	$R11(\Omega)$	$R22(\Omega)$	$R12(\text{K}\Omega)$
Model	221	221	21.7
Simulation	232	232	22.2

Table 5.1. Comparison of resistance values obtained from simulations and the scalable model for the example in Fig. 5.1.

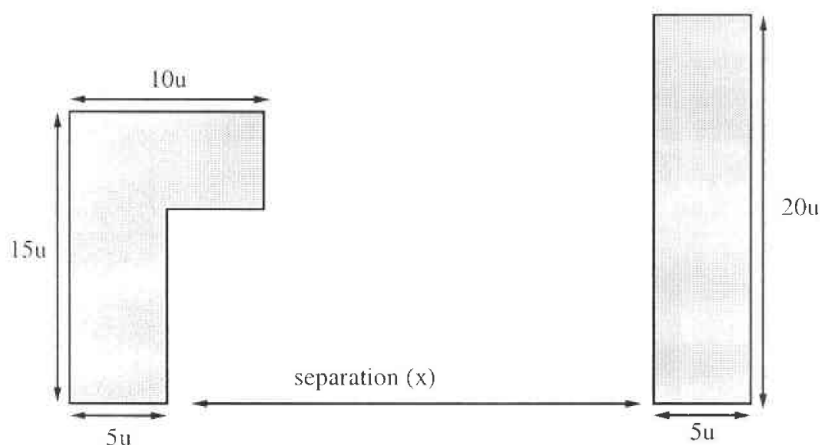


Figure 5.2. Verification of the model for different contact shapes for a separation $x = 40\mu\text{m}$.

	$R11(\Omega)$	$R22(\Omega)$	$R12(K\Omega)$
Model	252	294	10.96
Simulation	264	292	11.29

Table 5.2. Comparison of resistance values obtained from simulations and the scalable model for the example in Fig. 5.2.

between the macromodel and simulations. The maximum error from the simulations is under 8%.

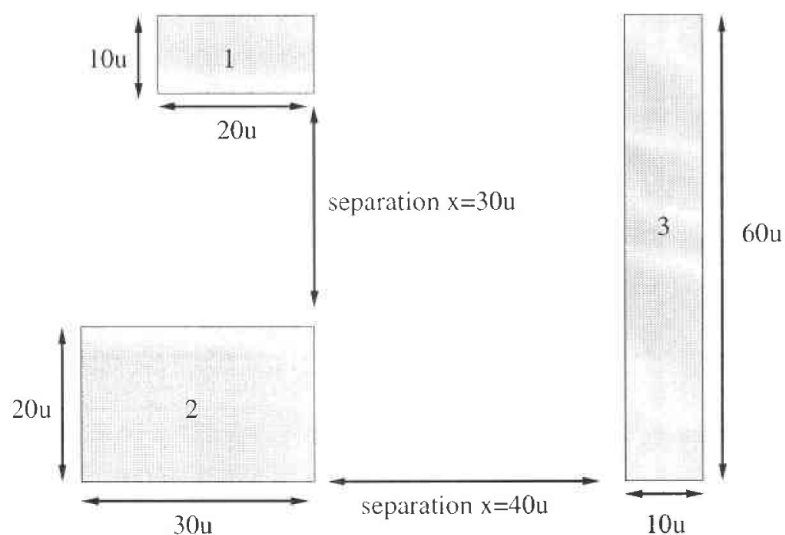


Figure 5.3. A three contact example is used to show the application of the scalable model to multiple contacts.

The traditional approaches divide the contacts into smaller panels before extracting the resistive network for the substrate. With the scalable model the resistance values can be directly extracted.

For the example of Fig. 5.1, consider each contact to be discretized into 10 smaller panels. The resulting Z matrix is a 20×20 dense matrix. The resistance

<i>Element</i>	<i>Model</i>	<i>Simulation</i>
R_{11}	249 Ω	261 Ω
R_{22}	139 Ω	141 Ω
R_{33}	109 Ω	118 Ω
R_{12}	6.9K Ω	7.3K Ω
R_{13}	21.4K Ω	22.4K Ω
R_{23}	14.4K Ω	14.2K Ω

Table 5.3. Resistance values from simulations and the scalable model are in good agreement for the example in Fig. 5.3.

values would be determined by inverting this dense matrix which has an order of complexity 20^3 if a direct method is used. The same calculation can be performed by using the scalable macromodel. In this case, only the inverse of a 2×2 matrix must be calculated.

Now consider a case of three contacts as shown in Fig. 5.4. The first contact is divided into n_1 panels, while the second and third contacts are divided into n_2 and n_3 panels, respectively. As a result of the contact discretization, the Z matrix will be a dense matrix of size $(n_1 + n_2 + n_3) \times (n_1 + n_2 + n_3)$. For the scalable approach the matrix size will be 3×3 . In a general case of K contacts, the Z matrix will be of size Z_{size} :

$$Z_{size} = \left(\sum_{i=1}^K n_i \right) \left(\sum_{i=1}^K n_i \right) \quad (5.1)$$

where n_i is the number of panels for the i^{th} contact. For comparison, with the scalable approach the Z matrix will only be of size $K \times K$ which is a significantly

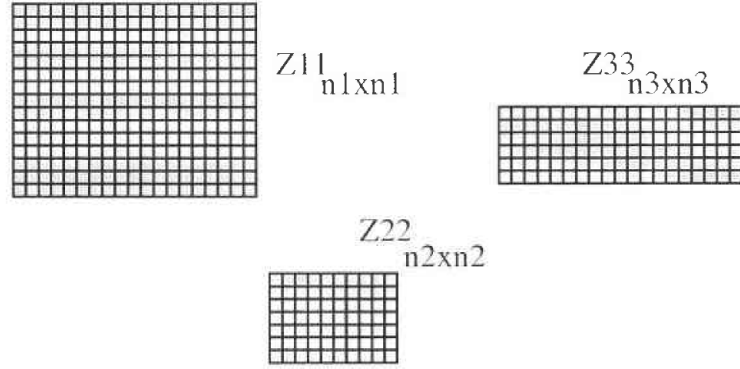


Figure 5.4. A non-scalable substrate model requires division of contacts into small panels.

smaller matrix. The scalability of the model with contact dimensions makes it computationally efficient. Therefore, the macromodel can handle problems with a large number of contacts.

Next, we provide a comparison of the efficiency of the scalable model with panel-based approaches. For the three given examples of application the computation complexities are compared in terms of the total number of panels, P . The Z matrix size is $P \times P$ and is summarized in Table 5.4. It is clear that the model is computationally much more efficient compared to approaches in which contacts are divided into smaller panels.

<i>Example</i>	<i>Model</i>	<i>Simulation</i>
Fig. 5.1	2×2	880×880
Fig. 5.2	2×2	395×395
Fig. 5.3	3×3	1267×1267

Table 5.4. Size of Z matrices for the scalable model and panel-based approaches.

Finally consider a realistic substrate extraction example from [4]. In this case there are 52 contacts that are discretized into 2647 panels for the Green's function approach. This results in a Z matrix of size 2647×2647 . In order to compute the resistance values iterative techniques such as GMRES or Krylov subspace methods are necessary. For this example, with the scalable macromodel the Z matrix is of size 52×52 . This is a significantly smaller matrix and the substrate resistances can be computed using direct matrix inversion.

6. EXPERIMENTAL VERIFICATION

The Z -parameter formulation model proposed in the previous sections has been validated on a test chip. This test chip was fabricated in a $0.35\mu\text{m}$ CMOS TSMC process through MOSIS. The chip has several substrate test structures as shown in Fig. 6.1. The test structures for validation of the low frequency scalable model have several $p+$ contacts of different sizes and shapes. All the contacts are connected to $60\mu\text{m} \times 60\mu\text{m}$ DC probe pads for probing. The measurement setup consists of a HP 4156B semiconductor parameter analyzer and a CASCADE probe station.

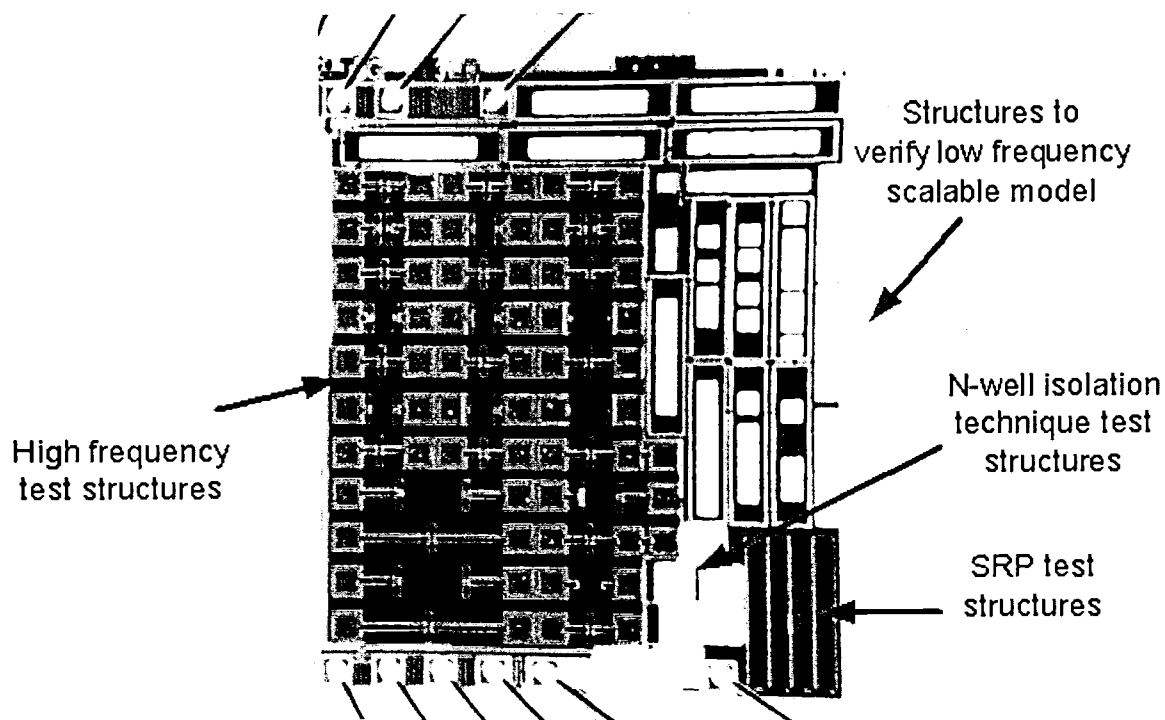


Figure 6.1. Substrate coupling test structures.

The chip has a downbond which makes an electrical connection from the package cavity to the bottom of the chip. This bonding finger is also connected (wired) to one of the chip's pads, therefore it was possible to ground the backplane by using a pin during the measurements. The backplane of the die is contacted to a down-bonding metal plate through the conductive epoxy. The contact between the substrate and the epoxy behaves as a nonlinear element. This nonlinearity has to be deembedded from the measurement results. The characterization of backplane nonlinearity is done by using the method in [6].

Fig. 6.2 shows measured Z_{11} values for different sized rectangular contacts. This figure verifies the proposed Z_{11} model.

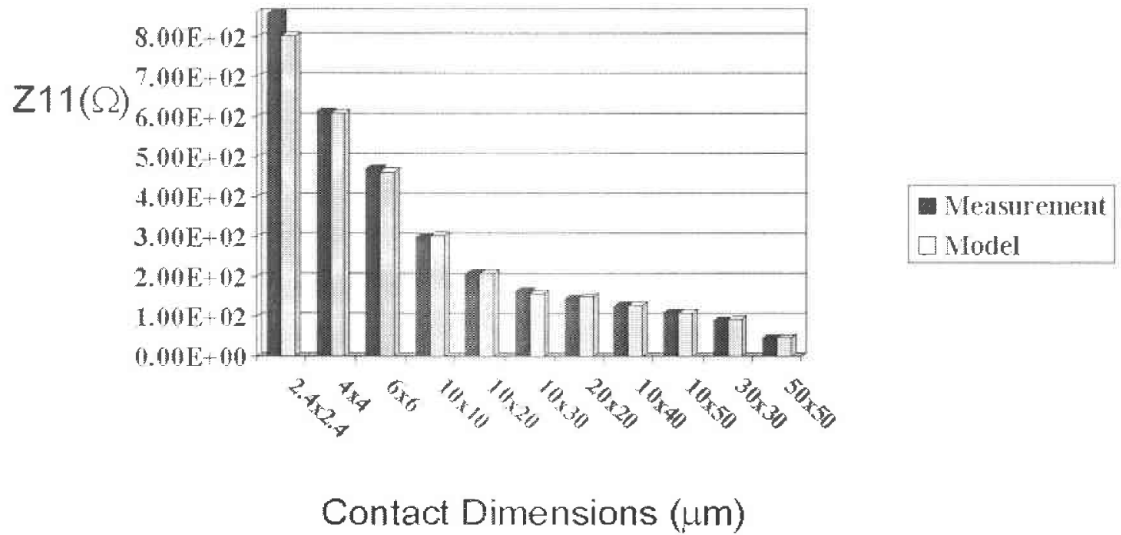


Figure 6.2. Measured data for Z_{11} agrees with the results obtained from the model.

$$Z_{11} = \frac{1}{K_1 Area + K_2 Perimeter + K_3} \quad (6.1)$$

In (6.1) curve fitting parameters for the measured Z_{11} values are

$$K_1 = 3.9157 \times 10^6 \left(\frac{1}{\Omega m^2} \right) \quad K_2 = 55.3087 \left(\frac{1}{\Omega m} \right) \quad K_3 = 6.9400 \times 10^{-4} \left(\frac{1}{\Omega} \right)$$

These are very close to the ones obtained from simulation results for the HP $0.5\mu m$ CMOS process. This is expected because both the HP $0.5\mu m$ and TSMC $0.35\mu m$ are heavily doped epi processes. Coefficients obtained for simulated data are:

$$K_1 = 3.1911 \times 10^6 \left(\frac{1}{\Omega m^2}\right) \quad K_2 = 47.6177 \left(\frac{1}{\Omega m}\right) \quad K_3 = 7.0579 \times 10^{-4} \left(\frac{1}{\Omega}\right)$$

This test chip includes different contact geometries along with the rectangular ones. Measurement results show that the area and perimeter dependent Z_{11} model also predicts the measured values accurately for these different shapes. Fig. 6.3 shows a L-shaped contact, an U-shaped contact and a square-shaped contact as examples. The area and perimeter for each contact is also shown in Fig. 6.3. The model agrees with the measurements for all three examples.

In order to measure Z_{12} values, an array of contacts with different separations is used. Fig. 6.4 (a) shows eight $2.4\mu m \times 2.4\mu m$ contacts with four different separations. Measurement results verify the exponential behavior of the Z_{12} model in Fig. 6.4 (b). The parameters obtained from measurements are

$$\alpha = 898.15\Omega \quad \beta = 8.676 \times 10^4 \frac{1}{m}$$

The simulated β value from Momentum and EPIC simulations for the HP $0.5\mu m$ CMOS process is around $8.3 \times 10^4 \frac{1}{m}$. The close agreement between the β values is expected since both the HP $0.5\mu m$ and TSMC $0.35\mu m$ are heavily doped processes and have similar doping profiles.

The α value can be also calculated from the model as a function of area and perimeter at zero separation. At zero separation the two contacts merge into a single contact. Fig. 6.5 shows the area and perimeter calculation of the resulting single contact.

By using the total area and perimeter values in Fig. 6.5, α can be calculated as:

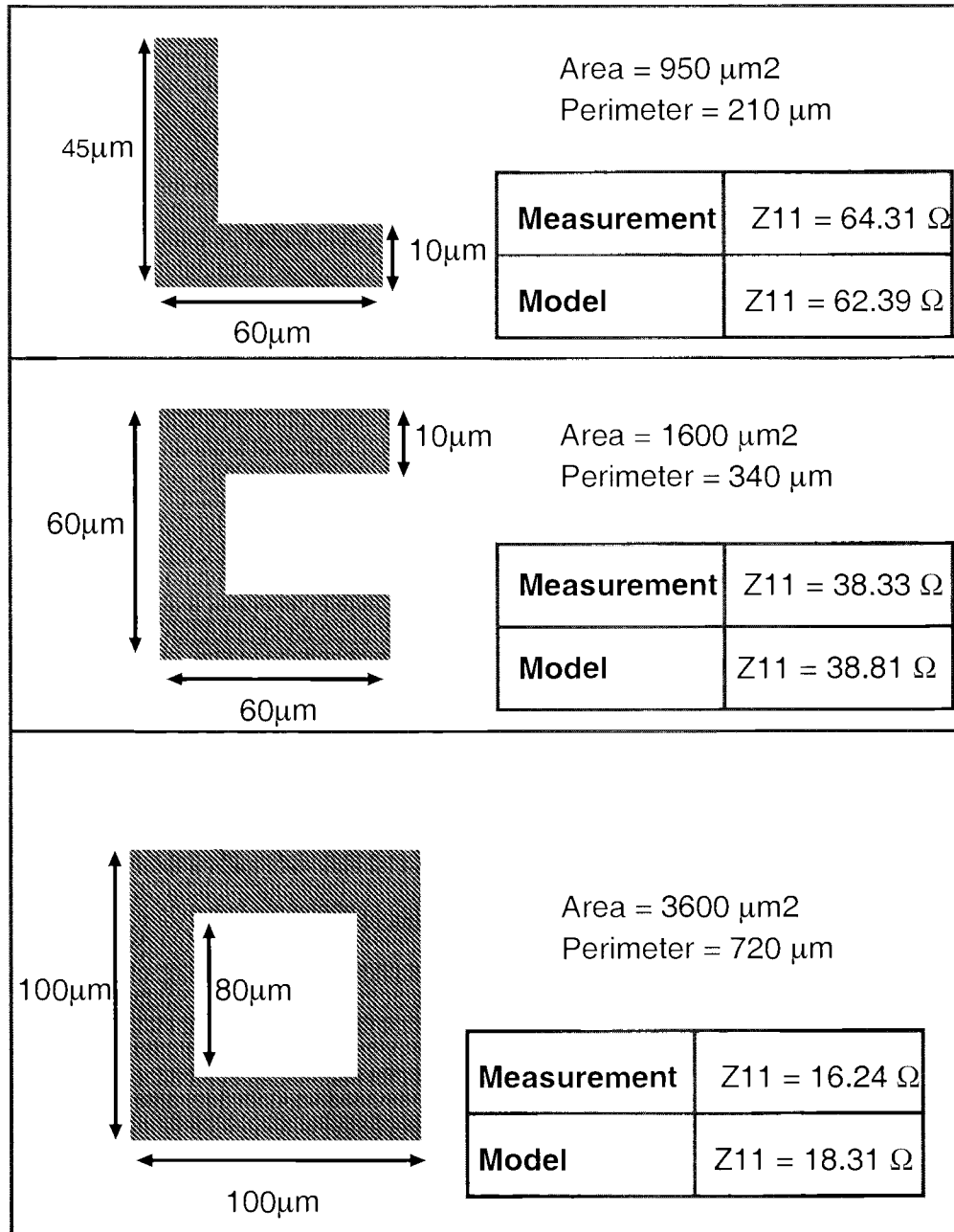
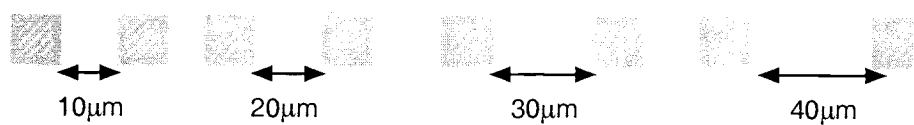
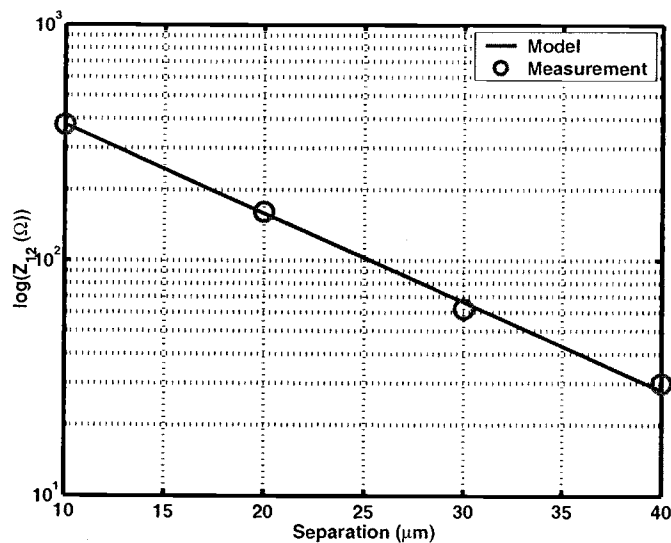


Figure 6.3. Different contact geometries. Measurement results show that the area and perimeter dependent Z_{11} model also predicts the measured values accurately for these different shapes.



(a)



(b)

Figure 6.4. (a) Array structure for $2.4\mu\text{m} \times 2.4\mu\text{m}$ contacts. (b) Z_{12} measurement results agree with the model for contacts of (a).

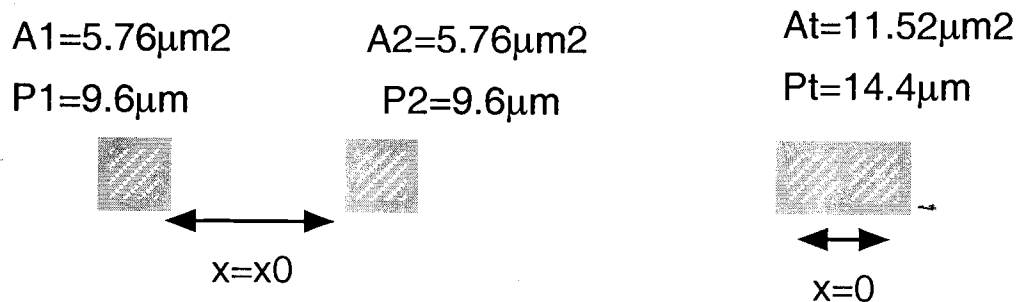


Figure 6.5. At zero separation the two $2.4\mu\text{m} \times 2.4\mu\text{m}$ contacts merge into a single contact of size $4.8\mu\text{m} \times 2.4\mu\text{m}$.

$$\alpha = \frac{1}{K_1 A_t + K_2 P_t + K_3} = 824.37\Omega \quad (6.2)$$

The α value obtained from model is in agreement with the measured value of 898.15 Ω .

the dependence of α on contact dimensions can also be verified with measurements. Fig. 6.6 shows three different sized pair of contacts at 10 μm separation. the values of α can be obtained from the ratio of $Z_{12}/\exp(-\beta \times 10\mu m)$ where $\beta = 8.676 \times 10^4$ 1/ m as measured for this process. A comparison of the obtained

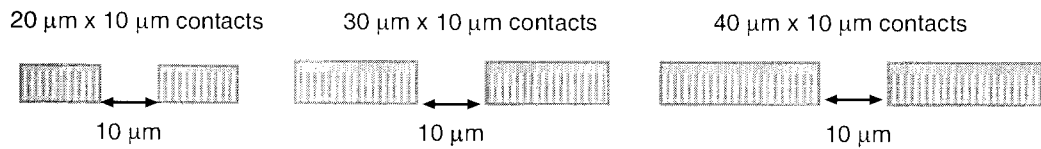


Figure 6.6. Three different sized contact pairs at a separation of 10 μm .

α values and the model is shown in Fig. 6.7. This example shows that the value of α is equal to the Z_{11} value of a single contact when the two contacts merge into one for zero separation.

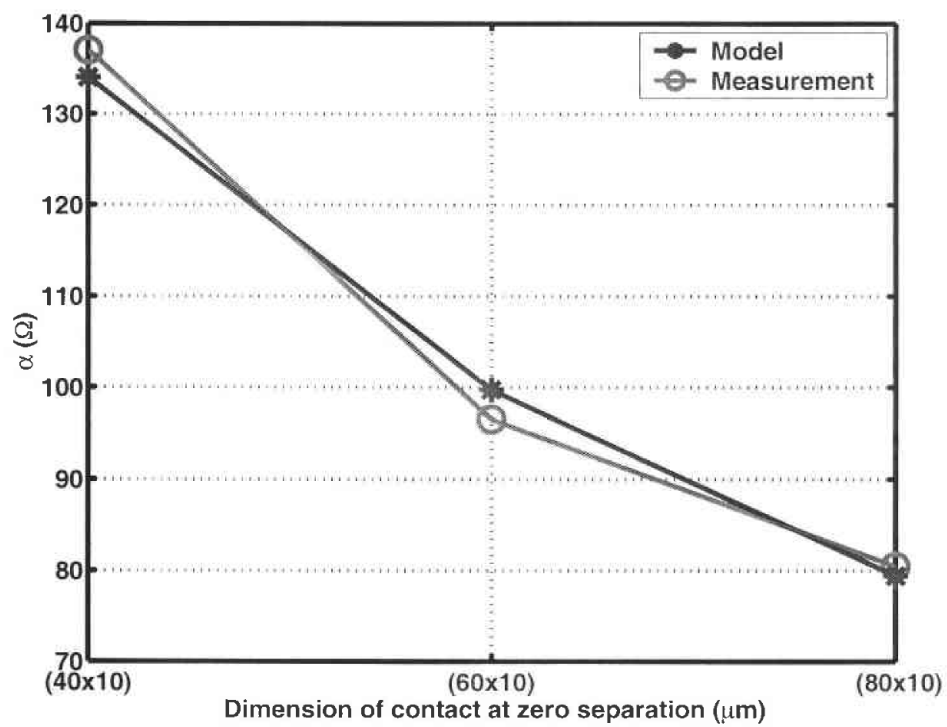


Figure 6.7. The modeled and extracted values of α are in good agreement.

7. CONCLUSION

This thesis presents an efficient and accurate modeling approach for substrate noise coupling analysis. The key to the efficiency and accuracy is a model that is scalable with both the geometry and the spacing of the contacts. The model was developed for heavily doped substrates and good agreement is achieved between the model, simulations and measurements. A preliminary model for lightly doped substrates is also proposed. The efficiency and accuracy of this model have been demonstrated on several examples. Future work will include completing the substrate noise coupling model in lightly doped substrates considering die area effects, incorporation of this model in a CAD tool and studying the applications of the model to circuit examples. One such circuit of interest is the oscillator. Substrate noise affects the phase noise and jitter in oscillators. This model is being used to predict the effect of substrate noise coupling on jitter in ring oscillators. Low noise amplifiers and data converters are some of the other circuits for which this model can be used.

BIBLIOGRAPHY

- [1] B. R. Stanistic, N. K. Verghese, R. A. Rutenbar, L. R. Carley and D. J. Allstot, "Addressing substrate coupling in mixed-mode IC's: simulations and power distribution synthesis," *IEEE Journal of Solid-State Circuits*, vol. 29, pp. 226-238, March 1994.
- [2] I. L. Wemple and A. T. Yang, "Integrated circuit substrate coupling models based on Voronoi-Tessellation substrate macromodels," *IEEE Trans. Computer-Aided Design*, pp. 1459-1469, December 1995.
- [3] R. Gharpurey and R. G. Meyer, "Modeling and analysis of substrate coupling in integrated circuits," *IEEE Journal of Solid-State Circuits*, vol. 31, no. 3, pp. 344-352, March 1996.
- [4] J. P. Costa, M. Chou and L. M. Silveria, "Efficient techniques for accurate modeling and simulation of substrate coupling in mixed-signal IC's," *IEEE Trans. Computer-Aided Design*, pp. 597-607, May 1999.
- [5] L. M. Silveria, M. Kamon and J. White, "Efficient reduced-order modeling of frequency-dependent coupling inductances associated with 3-D interconnect structures," *IEEE/ACM Proc. DAC*, pp. 376-380, June 1995.
- [6] A. Samavedam, A. Sadate, K. Mayaram and T. S. Fiez, "A scalable substrate noise coupling model for design of mixed-signal IC's," *IEEE Journal of Solid-State Circuits*, vol. 35, pp. 895-903, June 2000.
- [7] A. C. Sadate, "A substrate noise coupling model for lightly doped CMOS processes," M.S. Thesis, Oregon State University, December 2000.
- [8] D. K. Su, M. J. Loinaz, S. Masui and B. A. Wooley, "Experimental results and modeling techniques for substrate noise in mixed-signal integrated circuits," *IEEE Journal of Solid-State Circuits*, vol. 28, pp. 420-430, April 1993.
- [9] N. K. Verghese, D. J. Allstot and M. A. Wolfe, "Fast parasitic extraction for substrate coupling in mixed-signal ICs," *IEEE Custom Integrated Circuits Conference*, pp. 121-124, May 1995.
- [10] E. Charbon, R. Gharpurey, R. G. Meyer and A. Sangiovanni-Vincentelli, "Substrate optimization based on semi-analytical techniques," *IEEE Trans. Computer-Aided Design of Integrated Circuits and Systems*, vol. 18, no. 2, pp. 172-190, February 1999.
- [11] T. Smedes, N. P. van der Meijs and A. J. van Genderen, "Boundary element methods for 3D capacitance and substrate resistance calculations in inhomoge-

neous media in a VLSI layout verification package”, *Advances in Engineering Software*, vol. 20, no. 1, pp. 19-27, 1994.

- [12] A. J. Van Genderen and N. P. Van der Meijs, “Modeling substrate coupling effects using a layout-to-circuit extraction program,” *Proceedings of IEEE Benelux Workshop on Circuits, Systems and Signal Processing*, pp. 193-200, November 1997.
- [13] MEDICI, Version 2000.2.0, Avant! Corporation, 2000.
- [14] Agilent EEsof Momentum, Electromagnetic Design and Simulation, Advanced Design System 1.5, Agilent Technologies, December 2000.
- [15] Cheng-Gang Xu, “EPIC, Program for extraction of the resistance and capacitance of substrate with the Green’s Function method,” Oregon State University, 2001.
- [16] Affirma Substrate Coupling Analysis Version 4.4.5, Cadence Design Systems, Inc., December 1999.
- [17] N. K. Verghese and D. J. Allstot, “Computer-aided design considerations for mixed-signal coupling in RF integrated circuits,” *IEEE Journal of Solid-State Circuits*, vol. 33, no. 3, pp. 314-323, March 1998.

APPENDICES

APPENDIX A. Calculation of Z Parameters from S Parameters

The S and Y parameters for a 2-port network are given by:

$$\begin{aligned} b_1 &= S_{11}a_1 + S_{12}a_2 & i_1 &= Y_{11}V_1 + Y_{12}V_2 \\ b_2 &= S_{12}a_1 + S_{22}a_2 & i_2 &= Y_{12}V_1 + Y_{22}V_2 \end{aligned}$$

Substituting for a_{ij} and b_{ij} in terms of the port voltages and currents in the S -parameter equation

$$\frac{V_1 - Z_0 i_1}{2\sqrt{Z_0}} = S_{11} \left(\frac{V_1 + Z_0 i_1}{2\sqrt{Z_0}} \right) + S_{12} \left(\frac{V_2 + Z_0 i_2}{2\sqrt{Z_0}} \right) \quad (\text{A1})$$

$$\frac{V_2 - Z_0 i_2}{2\sqrt{Z_0}} = S_{21} \left(\frac{V_1 + Z_0 i_1}{2\sqrt{Z_0}} \right) + S_{22} \left(\frac{V_2 + Z_0 i_2}{2\sqrt{Z_0}} \right) \quad (\text{A2})$$

From (A1):

$$Z_0 i_1 + S_{11} Z_0 i_1 + S_{12} Z_0 i_2 = V_1 - S_{11} V_1 - S_{12} V_2$$

From (A2):

$$Z_0 i_2 + S_{21} Z_0 i_1 + S_{22} Z_0 i_2 = V_2 - S_{21} V_1 - S_{22} V_2$$

$$Z_0 \begin{bmatrix} S_{11} + 1 & S_{12} \\ S_{21} & S_{22} + 1 \end{bmatrix} \begin{bmatrix} i_1 \\ i_2 \end{bmatrix} = \begin{bmatrix} 1 - S_{11} & -S_{12} \\ -S_{21} & 1 - S_{22} \end{bmatrix} \begin{bmatrix} V_1 \\ V_2 \end{bmatrix}$$

$$\implies Z_0 (S + I) \begin{bmatrix} i_1 \\ i_2 \end{bmatrix} = (I - S) \begin{bmatrix} V_1 \\ V_2 \end{bmatrix}$$

$$\begin{bmatrix} i_1 \\ i_2 \end{bmatrix} = \frac{1}{Z_0} (S + I)^{-1} (I - S) \begin{bmatrix} V_1 \\ V_2 \end{bmatrix} = Y \begin{bmatrix} V_1 \\ V_2 \end{bmatrix}$$

So:

$$Y = \frac{1}{Z_0} (S + I)^{-1} (I - S)$$

$$Z = Y^{-1}$$

For the special case of two contacts the Z and Y parameters are related to each other as follows:

$$Z_{11} = \frac{Y_{22}}{|Y|}, \quad Z_{12} = \frac{-Y_{12}}{|Y|}, \quad Z_{21} = \frac{-Y_{21}}{|Y|}, \quad Z_{22} = \frac{Y_{11}}{|Y|}$$

APPENDIX B. Model parameter extraction for Z_{11}

PARAMETER EXTRACTION FLOW FOR Z_{11}

Z_{11} is measured for a single contact. It is the ratio of open circuit voltage at the contact to the input current at the contact, with all other contacts as open circuits.

$$Z_{11} = \frac{V_1}{I_1} \quad (B1)$$

Z_{11} can be modeled as a function of the contact area and perimeter.

$$Z_{11} = \frac{1}{K_1 \times Area + K_2 \times Perim + K_3} \quad (B2)$$

Parameters to extract: $K_1(\frac{1}{\Omega m^2})$, $K_2(\frac{1}{\Omega m})$ and $K_3(\frac{1}{\Omega})$. These parameters are constant for a given substrate.

Objective: To calculate Z_{11} for any contact size in a given substrate using the extracted parameters.

Parameter Extraction Steps:

- **Step 1:** Obtain at least 10 different data points (from simulations or measurements) for Z_{11} using a single contact with both square and rectangular geometries. Vary contact sizes in the range of $2.4\mu m$ to $100\mu m$.
- **Step 2:** Extract parameters K_1 , K_2 and K_3 by curve-fitting (B2) to Z_{11} data.

Extracted Parameter Values:

- **HP $0.5\mu m$ process:** Parameters from simulated data.

$$K_1 = 3.1911 \times 10^6 \left(\frac{1}{\Omega m^2}\right) \quad K_2 = 47.6177 \left(\frac{1}{\Omega m}\right) \quad K_3 = 7.0579 \times 10^{-4} \left(\frac{1}{\Omega}\right)$$

- **TSMC $0.35\mu m$ process:** Parameters from measured data.

$$K_1 = 3.9157 \times 10^6 \left(\frac{1}{\Omega m^2}\right) \quad K_2 = 55.3087 \left(\frac{1}{\Omega m}\right) \quad K_3 = 6.9400 \times 10^{-4} \left(\frac{1}{\Omega}\right)$$

```

clear all;
close all;
load newZ11.dat;
wx=newZ11(:,1);
wz=newZ11(:,2);
Z11=1./newZ11(:,3);

global count errvec

count=1;
errvec=[];

options(2)=1e-10;
options(3)=1e-10;
options(6)=2;
options(7)=1;
options(14)=50000;

lam=fmins('fitZ11xz',[3e6,40, 1e-4],options,[],wx,wz,Z11);

K1=lam(1);
K2=lam(2);
K3=lam(3);
y = (K1*(wx.*wz)+K2*2*(wx+wz)+K3);
grid on
plot(wx.*1e6,1./y,'b*',wx.*1e6,1./Z11,'ro');
hold on
plot(wx.*1e6,1./y,'b',wx.*1e6,1./Z11,'r');
xlabel('Dimension of source (\mum)');
ylabel('Z_{11} (\Omega)');
grid on;
legend('Model','Measurement')
figure
plot(wx*1e6,((1./y)-(1./Z11))./(1./Z11)*100);
title('Percentage error')
xlabel('Dimension of source (\mum)');
ylabel('Percentage error');
grid on;

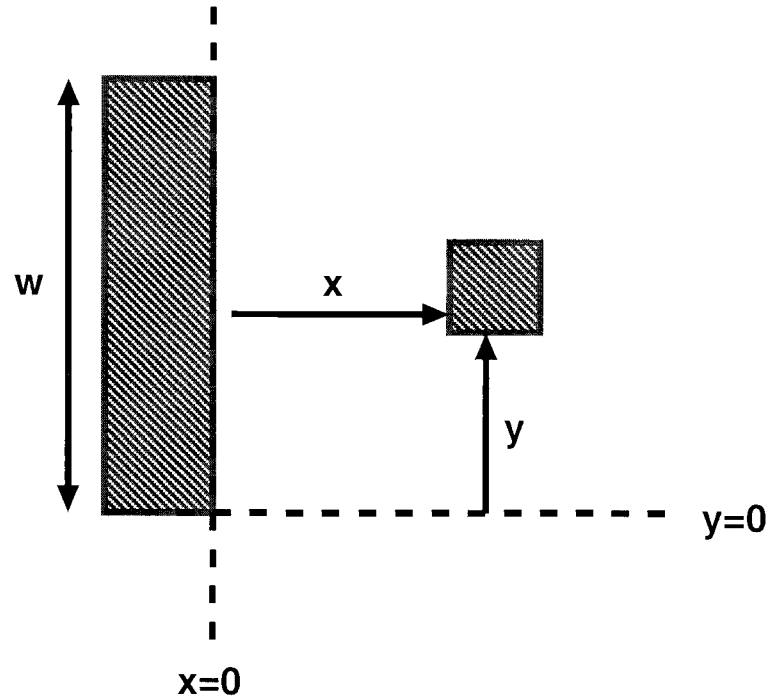
% Error calculation between simulated data and the model function.

```

```
function [error_data]=fitZ11xz(lam,wx,wz,Z11)
global errvec;
global count;
error = Z11-(lam(1)*(wx.*wz)+lam(2)*2*(wx+wz)+lam(3));
error_data=norm(error);
errvec(count)=error_data;
count = count+1;
```

APPENDIX C. Model parameter extraction for Z_{12}

$Z_{12}(x, y)$ is a function of both x and y , where x is the separation between the contacts and y is the relative position of the two contacts, as described below.



Z_{12} is measured for two contacts. It is the ratio of the open circuit voltage at the first contact to the input current at the second contact, with all other contacts as open circuits.

$$Z_{12} = \frac{V_1}{I_2} \Big|_{I_1=0}$$

PARAMETER EXTRACTION FLOW FOR Z_{12} (x dependence)
 Z_{12} as a function of x can be modeled as

$$Z_{12} = \alpha e^{-\beta x}$$

Parameter to extract: $\beta(\frac{1}{m})$. β is a constant for a given substrate.

Parameter to calculate: $\alpha(\Omega)$. α depends on contact dimensions.

Objective: To calculate Z_{12} for any contact size in a given substrate using extracted parameters.

Parameter Extraction Steps:

- **Step 1:** Obtain at least 10 different data points (from simulations or measurements) for Z_{12} using two contacts with square or rectangular geometries for different separations. First choose geometries in the range of $2.4\mu m$ to $100\mu m$ and then vary the separation from $10\mu m$ to $120\mu m$.
- **Step 2:** Two contacts merge into a single contact at zero separation. The value of α is equal to the Z_{11} value of the merged contact. Therefore the value of α can be calculated from:

$$\alpha = \frac{1}{K_1 \times Area + K_2 \times Perim + K_3}$$

where *Area* and *Perim* are the area and the perimeter of the merged contact, respectively.

- **Step 3:** Using the Z_{12} data and the expression for $Z_{12} = \alpha e^{-\beta x}$ curve fit to determine β .

Extracted Parameter Values:

- **HP $0.5\mu m$ process:** β from simulated data is

$$\beta = 8.3 \times 10^4 \left(\frac{1}{m}\right)$$

- **TSMC $0.35\mu m$ process:** β from measured data is

$$\beta = 8.676 \times 10^4 \left(\frac{1}{m}\right)$$

PARAMETER EXTRACTION FLOW FOR Z_{12} (y dependence)

Z_{12} as a function of y can be modeled as

$$Z_{12} = ay^2 + by + c$$

Parameters to extract: a ($\frac{\Omega}{m^2}$) and b ($\frac{\Omega}{m}$). Both parameters a and b scale with contact dimensions.

Parameter to calculate: $c(\Omega)$. c also depends on contact dimensions.

Objective: To calculate Z_{12} for any contact size in a given substrate using extracted parameters.

Parameter Extraction Steps:

- **Step 1:** Select any separation larger than $10\mu m$ (x_a).
- **Step 2:** Obtain at least 10 different data points (from simulations or measurements) for Z_{12} using two contacts with square or rectangular geometries for different y values. First choose the geometries in the range of $2.4\mu m$ to $100\mu m$ such that one of the contacts will be larger than the other one and then vary the y from $0\mu m$ to the length of the large contact.
- **Step 3:** Calculate c by observing that $Z_{12}|_{y=0} = c$. $Z_{12}|_{y=0} = ay^2 + by + c|_{y=0} = c$. Thus $c = Z_{12}|_{y=0} = \alpha e^{-\beta x_a}$.
- **Step 4:** Determine a and b by curve fitting Z_{12} data for different y values.
- **Step 5:** Once the parameters are extracted for a specific pair of contacts, parameters can be obtained for any contact size. When the contact dimensions change the new α value for the contact pair will be:

$$\alpha_{new} = \frac{1}{K_1 \times Area_{new} + K_2 \times Perim_{new} + K_3}$$

where $Area_{new}$ and $Perim_{new}$ are the area and the perimeter of the new merged contacts at zero separation. Z_{12} for different contact sizes can be calculated by scaling parameters a , b and c by $\frac{\alpha_{new}}{\alpha}$.

Extracted Parameter Values:

- **HP 0.5 μm process:** The parameter is obtained from simulated data for contact sizes of $100\mu m \times 10\mu m$ and $10\mu m \times 10\mu m$ at a separation $x_a = 10\mu m$.

$$a = -4.0139 \times 10^9 \left(\frac{\Omega}{m^2}\right) \quad b = 3.6125 \times 10^5 \left(\frac{\Omega}{m}\right) \quad c = 15.1332 \times 10^5 (\Omega)$$

```

% Curvefitting
close all;

load newtest2.dat;
x=newtest2(:,1);
Z12=abs(newtest2(:,3));
global count errvec
count=1;
errvec=[];
options(2)=1e-10;
options(3)=1e-10;
options(6)=2;
options(7)=1;
options(14)=50000;

lam=fmins('fitZ12',[1e5],options,[],x,Z12);

alpha=lam(1);
beta=lam(2);

y=(alpha.*exp(-beta.*x));
grid on
semilogy(x.*1e6,y,x.*1e6,Z12,'ro');
xlabel('Separation (\mum)');
ylabel('Z_{12} (\Omega)');
grid on

figure
plot(x,(y-Z12)./Z12*100);
title('Percentage error')
xlabel('Dimension of source (\mum)');
ylabel('Z_{12} (\Omega)');
grid on;

% Error calculation between the model and dat

function [error_data]=fitZ12(lam,x,Z12)
global errvec;
global count;
error = Z12-(lam(1)*exp(-lam(2).*x));
error_data=norm(error);
errvec(count)=error_data;

```

```

count = count+1;

% Curvefitting for Z12 dependence on y
close all;
clear all;
xa=input('Please enter the separation between the two contacts. xa(m):');
w=input('Please enter the length of the large contact. w(m):');
s=input('Please enter the length of the small contact. s(m):');
load eff_10x10_50x10_x030u.dat
x=eff_10x10_50x10_x030u(:,1);
Z12=eff_10x10_50x10_x030u(:,2);
c=eff_10x10_50x10_x030u(1,2);
global count errvec

count=1;
errvec=[];
options(2)=1e-10;
options(3)=1e-10;
options(6)=2;
options(7)=1;
options(14)=50000;

lam=fmins('fit_quad',[-1e8],options,[],x,w,s,c,Z12);

a=lam(1);
b=-a*(w-s);

y = a*x.^2+b*x+c;

grid on
plot(x.*1e6,y,x.*1e6,Z12,'ro');
xlabel('Position of small contact (\mum)');
ylabel('Z_{12} (\Omega)');
grid on;
figure
plot(x,(y-Z12)./(Z12)*100);
title('Percentage error')
xlabel('Position of small contact (\mum)');
ylabel('Z_{12} (\Omega)');
grid on;

% Error calculation between the simulated data and model

```



```
function [error_data]=fit_quad(lam,x,w,s,c,Z12)
global errvec;
global count;
error = Z12-(lam(1)*x.^2+(-(w-s)*lam(1))*x+c);
error_data=norm(error);
errvec(count)=error_data;
count = count+1;
```

APPENDIX D. Cadence Affirma Substrate Coupling Analysis

Steps to use Cadence SCA:

1. Define a substrate profile file.

Heavily doped substrates

```
File name:heavilysub.prof
LAYER Z1=0.0   Z2=300.0 RHO=0.0375
LAYER Z1=300.0 Z2=303.0 RHO=130
LAYER Z1=303.0 Z2=304.0 RHO=0.194
BACKPLANE NAME= BACKPLANE!
```

Lightly doped substrates

```
File name:lightlysub.prof
LAYER Z1=0.0   Z2=675.0 RHO=43.457
LAYER Z1=675.0 Z2=675.2 RHO=0.06839
BACKPLANE NAME= BACKPLANE!
```

2. Obtain the substrate port definitions through adjustments to the DIVA extraction rule file.

Adjustments in the rules file (HP 0.5 μ m process):

```
(ivIf
  (switch "extract?") then
    (scab =(geomOr "scab"))
    (laydie=(geomOr "laydie"))
  (diffEnclCont=(geomEnclose pdiff contact))
    ; Create dummy connection layers for scaBulk
    (scaVia = (geomEmpty))
    (scaCond = (geomEmpty))
  ; PRE on the guard ring and its substrate port image
  o_scaBulk=measureResistance(scaBulk "resistor ivpcell" 0.05 0.56
    "r"
    (distribute 8)
    (ignore >= 0.01)
  )
)
 geomConnect
  (via scaVia scaCond scaBulk)
  (via nwell2diff nwell diff scaBulk)
  (via contact diff metalli scaBulk)
  (via laydie psubstr diff scaBulk)
```

```

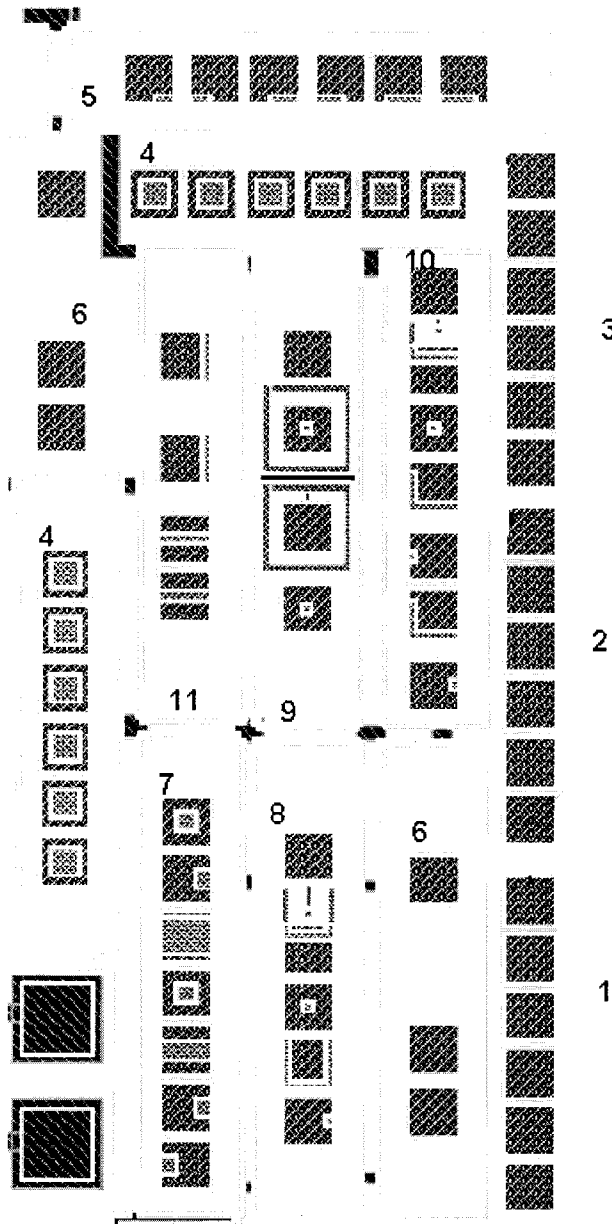
)

x=lambda( (ids2)
let( ( subLayers subResCV)
if( ids2->extracted then
subLayers = list(list("scab" 0.3 ) )
subResCV =list("analogLib" "presistor" "symbol")
subDieLpp=list("laydie" "drawing")
dbReplaceProp(ids2->extracted "subLayers"
               "ilList" subLayers)
dbReplaceProp(ids2->extracted "subResCellView"
               "ilList" subResCV)
dbReplaceProp(ids2->extracted "subDieLpp"
               "ilList" subDieLpp)
)
)
)
ivCallProc(x)
)
(saveInterconnect
  (scaBulk "scab" )
)

```

3. Run DIVA extraction in flat extraction mode.
4. In Virtuoso, select Verify-SCA from the extracted view. The generated substrate model is stored as res.out

APPENDIX E. Measurement Structures on the Test Chip

**Array 1 & 2:**

Array of $2.4\mu\text{m} \times 2.4\mu\text{m}$ contacts for small separations. The measurement results for this array is shown in Fig. 6.4.

Array 3:

Array of $6\mu m \times 6\mu m$ contacts.

Array 4:

Array of $30\mu m \times 30\mu m$ contacts.

Array 5:

Different contact sizes are at $10\mu m$ separation, in order to see the effect of contact dimensions on α . The measurement results for this array are shown in Fig. 6.7.

Array 6:

Three contacts of sizes $60\mu m \times 1.2\mu m$, $120\mu m \times 1.2\mu m$ and $180\mu m \times 1.2\mu m$ are included in this array. The objective is to see how Z_{11} changes if we change both contact area and perimeter by the same factor (2 and 3) for this example.

<i>Contact size (μm)</i>	<i>Measured $Z_{11}(\Omega)$</i>	<i>Z_{11} from Model(Ω)</i>
$60\mu m \times 1.2\mu m$	133.5279	129.1036
$120\mu m \times 1.2\mu m$	72.8195	68.1910
$180\mu m \times 1.2\mu m$	50.0573	46.3313

Array 7:

These different sized rectangular contacts are used for Z_{11} measurements. Results are shown in Fig. 6.2. This array also includes an example of two different contact sizes for different y values. Contact sizes are $20\mu m \times 60\mu m$ and $20\mu m \times 20\mu m$.

Array 8:

Z_{11} measurement for the U-shaped contact included in this array is shown in Fig. 6.3.

Array 9:

Z_{11} measurement for the square-shaped contact included in this array is shown in Fig. 6.3.

Array 10:

Z_{11} measurement for the L-shaped contact included in this array is shown in Fig. 6.3.

Array 11:

The objective for the structures in this array is to see the effects of contact orientation on Z_{12} . Two vertically aligned and two horizontally aligned $60\mu m \times 10\mu m$ contacts with a separation of $54\mu m$ were used.

Array 3, Array 4, Array 7 and Array 11 have very small values of Z_{12} and reliable measurements could not be made. These structures are better suited to lightly doped substrates.